# CHAPTER 10

# TRAVELING WAVE AND BROADBAND ANTENNAS

## 10.1 INTRODUCTION

In the previous chapters we have presented the details of classical methods that are used to analyze the radiation characteristics of some of the simplest and most common forms of antennas (i.e., infinitely thin linear and circular wires, broadband dipoles and arrays). In practice there is a myriad of antenna configurations, and it would be almost impossible to consider all of them in this book. In addition, many of these antennas have bizzare types of geometries and it would be almost impractical, if not even impossible, to investigate each in detail. However, the general performance behavior of some of them will be presented in this chapter with a minimum of analytical formulations. Today, comprehensive analytical formulations are available for most of them, but they would require so much space that it would be impractical to include them in this book.

## 10.2 TRAVELING WAVE ANTENNAS

In Chapter 4, center-fed linear wire antennas were discussed whose amplitude current distribution was

1. constant for infinitesimal dipoles ($l \leq \lambda/50$)
2. linear (triangular) for short dipoles ($\lambda/50 < l \leq \lambda/10$)
3. sinusoidal for long dipoles ($l > \lambda/10$)

In all cases the phase distribution was assumed to be constant. The sinusoidal current distribution of long open-ended linear antennas is a standing wave constructed by two waves of equal amplitude and 180° phase difference at the open-end traveling in opposite directions along its length. The voltage distribution has also a standing wave pattern except that it has maxima (loops) at the end of the line instead of nulls (nodes) as the current. In each pattern, the maxima and minima repeat every integral number of half-wavelengths. There is also a $\lambda/4$ spacing between a null and a maximum in each of the wave patterns. The current and voltage distributions on open-ended wire antennas are similar to the standing wave patterns on open-ended transmission lines.

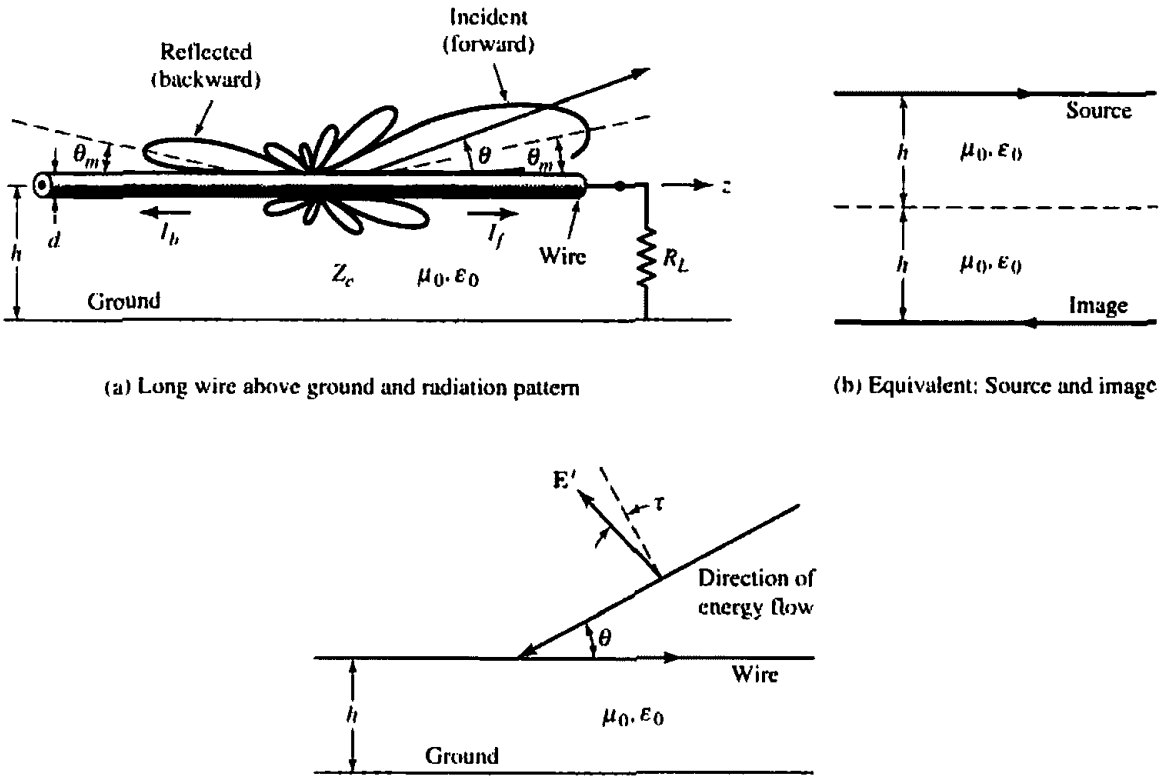


(a) Long wire above ground and radiation pattern

(b) Equivalent: Source and image

(c) Wave tilt

**Figure 10.1** Beverage (long-wire) antenna above ground.

Linear antennas that exhibit current and voltage standing wave patterns formed by reflections from the open end of the wire are referred to as *standing wave* or *resonant* antennas.

Antennas can be designed which have traveling wave (uniform) patterns in current and voltage. This can be achieved by properly terminating the antenna wire so that the reflections are minimized if not completely eliminated. An example of such an antenna is a long wire that runs horizontal to the earth, as shown in Figure 10.1. The input terminals consist of the ground and one end of the wire. This configuration is known as *Beverage or wave antenna.* There are many other configurations of traveling wave antennas. In general, all antennas whose current and voltage distributions can be represented by one or more traveling waves, usually in the same direction, are referred to as *traveling wave* or *nonresonant* antennas. A progressive phase pattern is usually associated with the current and voltage distributions.

Standing wave antennas, such as the dipole, can be analyzed as traveling wave antennas with waves propagating in opposite directions (forward and backward) and represented by traveling wave currents $I_f$ and $I_b$ in Figure 10.1(a). Besides the long wire antenna there are many examples of traveling wave antennas such as dielectric rod (polyrod), helix, and various surface wave antennas. Aperture antennas, such as reflectors and horns, can also be treated as traveling wave antennas. In addition, arrays of closely spaced radiators (usually less than $\lambda/2$ apart) can also be analyzed as traveling wave antennas by approximating their current or field distribution by a continuous traveling wave. Yagi-Uda, log-periodic, and slots and holes in a waveguide are some examples of discrete-element traveling wave antennas. In general, a traveling wave antenna is usually one that is associated with radiation from a continuous source. An excellent book on traveling wave antennas is one by C. H. Walter [1].

A traveling wave may be classified as a *slow* wave if its phase velocity $v_p$ ($v_p = \omega/k$, $\omega$ = wave angular frequency, $k$ = wave phase constant) is equal or smaller than the velocity of light $c$ in free-space ($v_p/c \leq 1$). A fast wave is one whose phase velocity is greater than the speed of light ($v_p/c > 1$).

In general, there are two types of traveling wave antennas. One is the *surface wave* antenna defined as "an antenna which radiates power flow from discontinuities in the structure that interrupt a bound wave on the antenna surface."* A surface wave antenna is, in general, a slow wave structure whose phase velocity of the traveling wave is equal to or less than the speed of light in free-space ($v_p/c \leq 1$).

For slow wave structures radiation takes place only at nonuniformities, curvatures, and discontinuities. Discontinuities can be either discrete or distributed. One type of discrete discontinuity on a surface wave antenna is a transmission line terminated in an unmatched load, as shown in Figure 10.1(a). A distributed surface wave antenna can be analyzed in terms of the variation of the amplitude and phase of the current along its structure. In general, power flows parallel to the structure, except when losses are present, and for plane structures the fields decay exponentially away from the antenna. Most of the surface-wave antennas are endfire or near-endfire radiators. Practical configurations include line, planar surface, curved, and modulated structures.

Another traveling wave antenna is a *leaky-wave* antenna defined as "an antenna that couples power in small increments per unit length, either continuously or discretely, from a traveling wave structure to free-space"† Leaky-wave antennas continuously lose energy due to radiation, as shown in Figure 10.2 by a slotted rectangular waveguide. The fields decay along the structure in the direction of wave travel and increase in others. Most of them are fast wave structures.

### 10.2.1 Long Wire

An example of a slow wave traveling antenna is a long wire, as shown in Figure 10.1. An antenna is usually classified as a *long* wire antenna if it is a straight conductor with a length from one to many wavelengths. A long wire antenna has the distinction of being the first traveling wave antenna.

The long wire of Figure 10.1(a), in the presence of the ground, can be analyzed approximately using the equivalent of Figure 10.1(b) where an image is introduced to take into account the presence of the ground. The magnitude and phase of the image are determined using the reflection coefficient for horizontal polarization as given by (4-129). The height $h$ of the antenna above the ground must be chosen so that the reflected wave (or wave from the image), which includes the phase due to reflection is in phase with the direct wave at the angles of desired maximum radiation. However, for typical electrical constitutive parameters of the earth, and especially for observation angles near grazing, the reflection coefficient for horizontal polarization is approximately $-1$. Therefore the total field radiated by the wire in the presence of the ground can be found by multiplying the field radiated by the wire in free space by the array factor of a two-element array, as was done in Section 4.8.2 and represented by (4-130).

The objective now is to find the field radiated by the long wire in free space. This is accomplished by referring to Figure 10.3. As the wave travels along the wire from the source toward the load, it continuously leaks energy. This can be represented by

*"IEEE Standard Definitions of Terms for Antennas" (IEEE Std 145-1983), *IEEE Trans. Antennas and Propagat.*, Vol. AP-31, No. 6, Part II, Nov. 1983.

†Ibid.

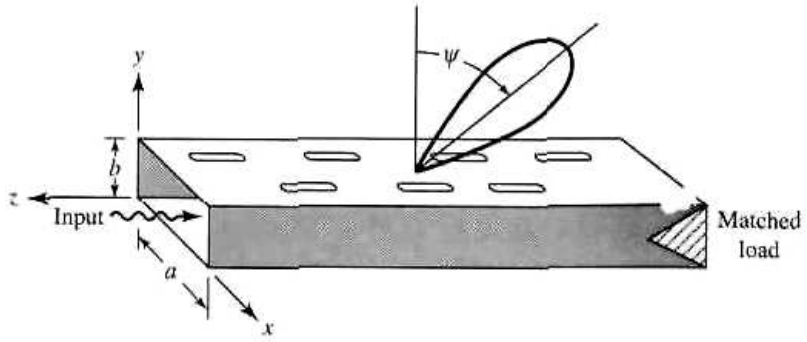


(a) Upper wall—longitudinal

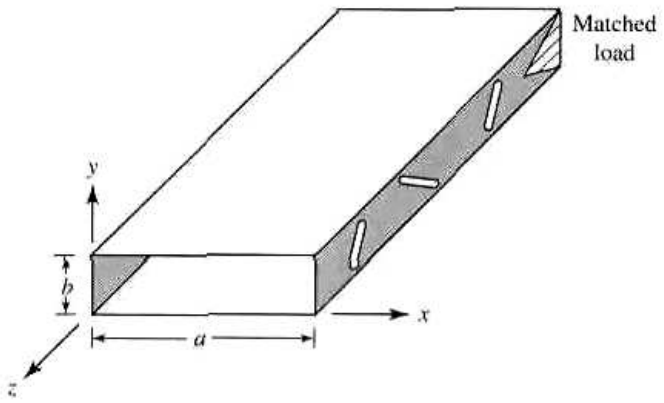


(b) Sidewall—inclined

**Figure 10.2** Leaky-wave waveguide slots; upper (broad) and side (narrow) walls.

an attenuation coefficient. Therefore the current distribution of the forward traveling wave along the structure can be represented by

$$\mathbf{I}_f = \hat{\mathbf{a}}_z I_z(z')e^{-\gamma(z')z'} = \hat{\mathbf{a}}_z I_0 e^{-[\alpha(z')+jk_z(z')]z'} \tag{10-1}$$

where $\gamma(z')$ is the propagation coefficient [$\gamma(z') = \alpha(z') + jk_z(z')$ where $\alpha(z')$ is the attenuation constant (nepers/meter) while $k_z(z')$ is the phase constant (radians/meter) associated with the traveling wave]. In addition to the losses due to leakage, there are wire and ground losses. The attenuation factor $\alpha(z')$ can also be used to take into account the ohmic losses of the wire as well as ground losses. However, these, especially the ohmic losses, are usually very small and for simplicity are neglected. In addition, when the radiating medium is air, the loss of energy in a long wire ($l \gg \lambda$) due to leakage is also usually very small, and it can also be neglected. Therefore the current distribution of (10-1) can be approximated by

$$\mathbf{I} = \hat{\mathbf{a}}_z I(z')e^{-jk_z z'} = \hat{\mathbf{a}}_z I_0 e^{-jk_z z'} \tag{10-1a}$$

where $I(z') = I_0$ is assumed to be constant. Using techniques outlined and used in Chapter 4, it can be easily shown that in the far-field

$$E_r \simeq E_\phi = H_r = H_\theta = 0 \tag{10-2a}$$

$$E_\theta \simeq j\eta \frac{klI_0 e^{-jkr}}{4\pi r} e^{-j(kl/2)(K-\cos\theta)} \sin\theta \frac{\sin[(kl/2)(\cos\theta - K)]}{(kl/2)(\cos\theta - K)} \tag{10-2b}$$

$$H_\phi \simeq \frac{E_\theta}{\eta} \tag{10-2c}$$

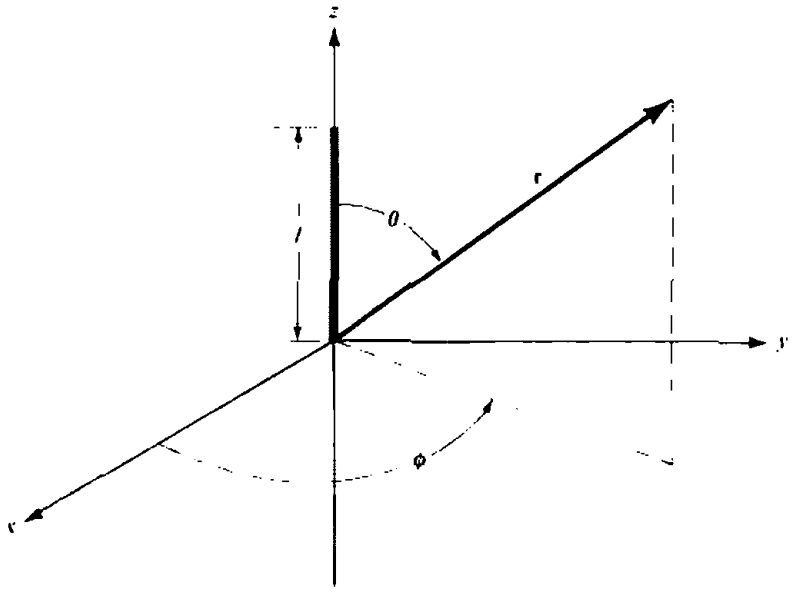


**Figure 10.3** Long wire antenna.

where $K$ is used to represent the ratio of the phase constant of the wave along the transmission line ($k_z$) to that of free-space ($k$), or

$$K = \frac{k_z}{k} = \frac{\lambda}{\lambda_g} \tag{10-3}$$

$\lambda_g$ = wavelength of the wave along the transmission line

Assuming a perfect electric conductor for the ground, the total field for Figure 10.1(a) is obtained by multiplying each of (10-2a)–(10-2c) by the array factor sin ($kh$ sin $\theta$).

For $k_z = k$ ($K = 1$) the time-average power density can be written as

$$\mathbf{W}_{av} = \mathbf{W}_{rad} = \hat{\mathbf{a}}_r \eta \frac{|I_0|^2}{8\pi^2 r^2} \frac{\sin^2\theta}{(\cos\theta - 1)^2} \sin^2\left[\frac{kl}{2}(\cos\theta - 1)\right] \tag{10-4}$$

which reduces to

$$\mathbf{W}_{av} = \mathbf{W}_{rad} = \hat{\mathbf{a}}_r \eta \frac{|I_0|^2}{8\pi^2 r^2} \cot^2\left(\frac{\theta}{2}\right) \sin^2\left[\frac{kl}{2}(\cos\theta - 1)\right] \tag{10-5}$$

From (10-5) it is evident that the power distribution of a wire antenna of length $l$ is a multilobe pattern whose number of lobes depend upon its length. Assuming that $l$ is very large such that the variations in the sine function of (10-5) are more rapid than those of the cotangent, the peaks of the lobes occur approximately when

$$\sin^2\left[\frac{kl}{2}(\cos\theta - 1)\right]_{\theta=\theta_m} = 1 \tag{10-6}$$

or

$$\frac{kl}{2}(\cos\theta_m - 1) = \pm\left(\frac{2m+1}{2}\right)\pi, \qquad m = 0, 1, 2, 3, \ldots \tag{10-6a}$$

The angles where the peaks occur are given by

$$\theta_m = \cos^{-1}\left[1 \pm \frac{\lambda}{2l}(2m + 1)\right], \qquad m = 0, 1, 2, 3, \ldots \tag{10-7}$$

The angle where the maximum of the major lobe occurs is given by $m = 0$ (or $2m + 1 = 1$). As $l$ becomes very large ($l \gg \lambda$) the angle of the maximum of the major lobe approaches zero degrees and the structure becomes a near endfire array.

In finding the values of the maxima, the variations of the cotangent term in (10-5) were assumed to be negligible (as compared to those of the sine term). If the effects of the cotangent term were to be included, then the values of the $2m + 1$ term in (10-7) should be

$$2m + 1 = 0.742, 2.93, 4.96, 6.97, 8.99, 11, 13, \ldots \tag{10-8}$$

(instead of 1, 3, 5, 7, 9, ...) for the first, second, third, and so forth maxima. The approximate values approach those of the exact for the higher order lobes.

In a similar manner, the nulls of the pattern can be found and occur when

$$\sin^2\left[\frac{kl}{2}(\cos\theta - 1)\right]_{\theta=\theta_n} = 0 \tag{10-9}$$

or

$$\frac{kl}{2}(\cos\theta_n - 1) = \pm n\pi, \qquad n = 1, 2, 3, 4, \ldots \tag{10-9a}$$

The angles where the nulls occur are given by

$$\theta_n = \cos^{-1}\left(1 \pm n\frac{\lambda}{l}\right), \qquad n = 1, 2, 3, 4, \ldots \tag{10-10}$$

for the first, second, third, and so forth nulls.

The total radiated power can be found by integrating (10-5) over a closed sphere of radius $r$ and reduces to

$$P_{\text{rad}} = \oiint_S \mathbf{W}_{\text{rad}} \cdot d\mathbf{s} = \frac{\eta}{4\pi}|I_0|^2\left[1.415 + \ln\left(\frac{kl}{\pi}\right) - C_i(2kl) + \frac{\sin(2kl)}{2kl}\right] \tag{10-11}$$

where $C_i(x)$ is the cosine integral of (4-68a). The radiation resistance is then found to be

$$\boxed{R_r = \frac{2P_{\text{rad}}}{|I_0|^2} = \frac{\eta}{2\pi}\left[1.415 + \ln\left(\frac{kl}{\pi}\right) - C_i(2kl) + \frac{\sin(2kl)}{2kl}\right]} \tag{10-12}$$

Using (10-5) and (10-11) the directivity can be written as

$$\boxed{D_0 = \frac{4\pi U_{\max}}{P_{\text{rad}}} = \frac{2\cot^2\left[\frac{1}{2}\cos^{-1}\left(1 - \frac{0.371\lambda}{l}\right)\right]}{1.415 + \ln\left(\frac{2l}{\lambda}\right) - C_i(2kl) + \frac{\sin(2kl)}{2kl}}} \tag{10-13}$$

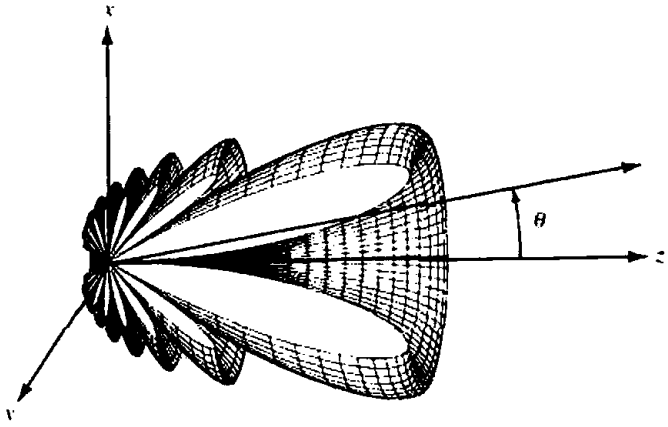


(a) Traveling wave

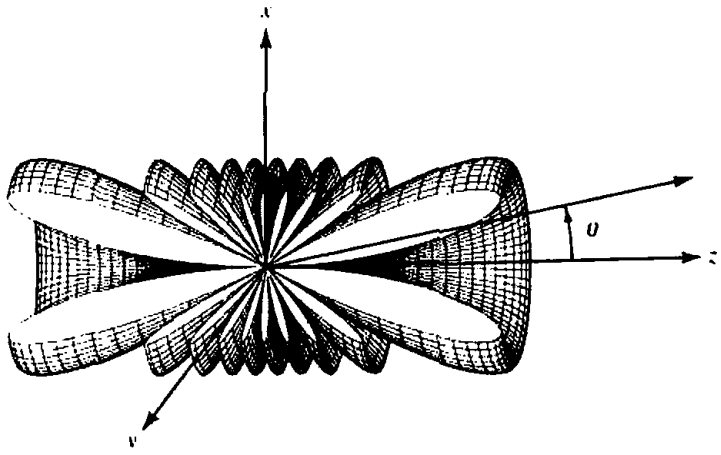


(b) Standing wave

**Figure 10.4** Three-dimensional free-space amplitude pattern for traveling and standing wave wire antennas of $l = 5\lambda$.

*A. Amplitude Patterns, Maxima, and Nulls*

To verify some of the derivations and illustrate some of the principles, a number of computations were made. Shown in Figure 10.4(a) is the three-dimensional pattern of a traveling wire antenna with length $l = 5\lambda$ while in Figure 10.4(b) is the three-dimensional pattern for a standing wave wire antenna with length $l = 5\lambda$. The corresponding two- dimensional patterns are shown in Figure 10.5. The pattern of Figure 10.4(a) is formed by the forward traveling wave current $I_f = I_1 e^{-jkz}$ of Figure 10.1(a) while that of Figure 10.4(b) is formed by the forward $I_f$ plus backward $I_b$ traveling wave currents of Figure 10.1(a). The two currents $I_f$ and $I_b$ together form a standing wave; that is, $I_s = I_f + I_b = I_1 e^{-jkz} - I_2 e^{+jkz} = -2jI_0 \sin(kz)$ when $I_2 = I_1 = I_0$. As expected, for the traveling wave antenna of Figure 10.4(a) there is maximum radiation in the forward direction while for the standing wave antenna of Figure 10.4(b) there is maximum radiation in the forward and backward directions. The lobe near the axis of the wire in the directions of travel is the largest. The magnitudes of the other lobes from the main decrease progressively, with an envelope proportional to $\cot^2(\theta/2)$, toward the other direction. The traveling wave antenna is used when it is desired to radiate or receive predominantly from one direction. As the length of the wire increases, the maximum of the main lobe shifts closer toward the axis and the number of lobes increase. This is illustrated in Figure 10.6 for a traveling

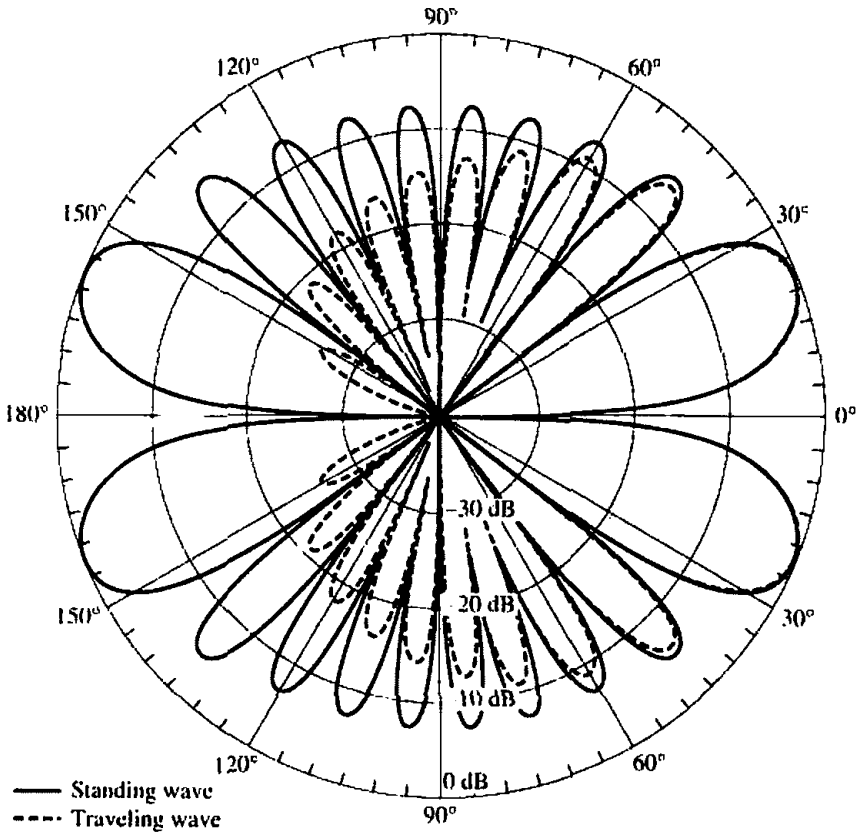


**Figure 10.5** Two-dimensional free-space amplitude pattern for traveling and standing wave wire antennas of $l = 5\lambda$.

wave wire antenna with $l = 5\lambda$ and $10\lambda$. The angles of the maxima of the first four lobes, computed using (10-8), are plotted in Figure 10.7(a) for $0.5\lambda \leq l \leq 10\lambda$. The corresponding angles of the first four nulls, computed using (10-10), are shown in Figure 10.7(b) for $0.5\lambda \leq l \leq 10\lambda$. These curves can be used effectively to design long wires when the direction of the maximum or null is desired.

*B. Input Impedance*

For traveling wave wire antennas the radiation in the opposite direction from the maximum is suppressed by reducing, if not completely eliminating, the current reflected from the end of the wire. This is accomplished by increasing the diameter of the wire or more successfully by properly terminating it to the ground, as shown in Figure 10.1. Ideally a complete elimination of the reflections (perfect match) can only be accomplished if the antenna is elevated only at small heights (compared to the wavelength) above the ground, and it is terminated by a resistive load. The value of the load resistor, to achieve the impedance match, is equal to the characteristic impedance of the wire near the ground (which is found using image theory). For a wire with diameter $d$ and height $h$ above the ground, an approximate value of the termination resistance is obtained from

$$R_L = 138 \log_{10}\left(4\frac{h}{d}\right) \tag{10-14}$$

To achieve a reflection-free termination, the load resistor can be adjusted about this value (usually about 200–300 ohms) until there is no standing wave on the antenna

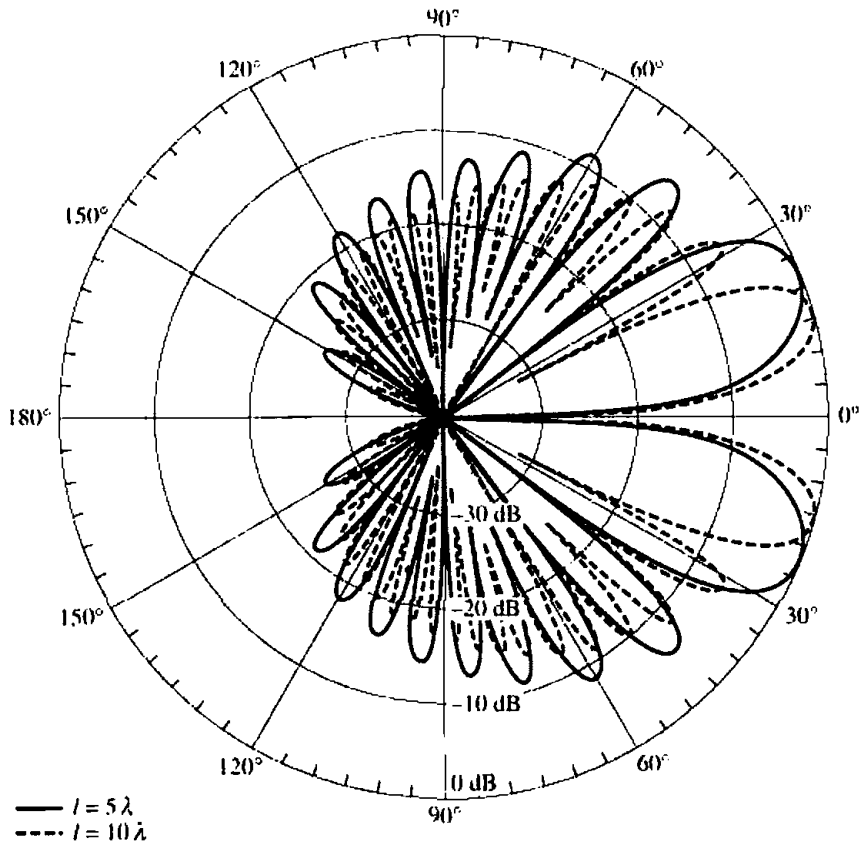


**Figure 10.6** Two-dimensional free-space amplitude pattern for traveling wave wire antenna of $l = 5\lambda$ and $10\lambda$.

wire. Therefore the input impedance is the same as the load impedance or the characteristic impedance of the line, as given by (10-14).

If the antenna is not properly terminated, waves reflected from the load traveling in the opposite direction from the incident waves create a standing wave pattern. Therefore the input impedance of the line is not equal to the load impedance. To find the input impedance, the transmission line impedance transfer equation of (9-18) can be used. Doing this we can write that the impedance at the input terminals of Figure 10.1(a) is

$$Z_{in}(l) = Z_c \left[ \frac{R_L + jZ_c \tan(\beta l)}{Z_c + jR_L \tan(\beta l)} \right] \tag{10-15}$$

*C. Polarization*

A long wire antenna is linearly polarized, and it is always parallel to the plane formed by the wire and radial vector from the center of the wire to the observation point. The direction of the linear polarization is not the same in all parts of the pattern, but it is perpendicular to the radial vector (and parallel to the plane formed by it and the wire). Thus the wire antenna of Figure 10.1, when its height above the ground is small compared to the wavelength and its main beam is near the ground, is not an effective element for horizontal polarization. Instead it is usually used to transmit or receive waves that have an appreciable vector component in the vertical plane. This is what is known as a *Beverage antenna* which is used more as a receiving rather than a transmitting element because of its poor radiation efficiency due to power absorbed in the load resistor.

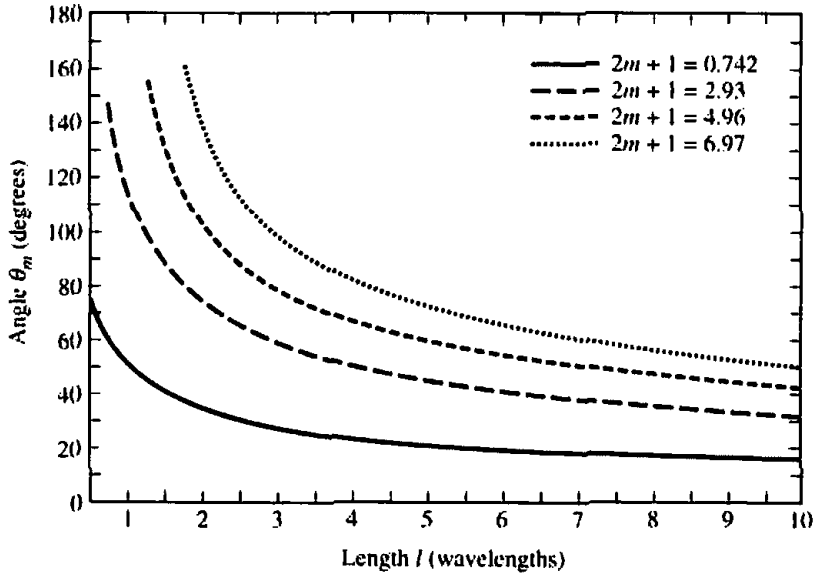


(a) Maxima

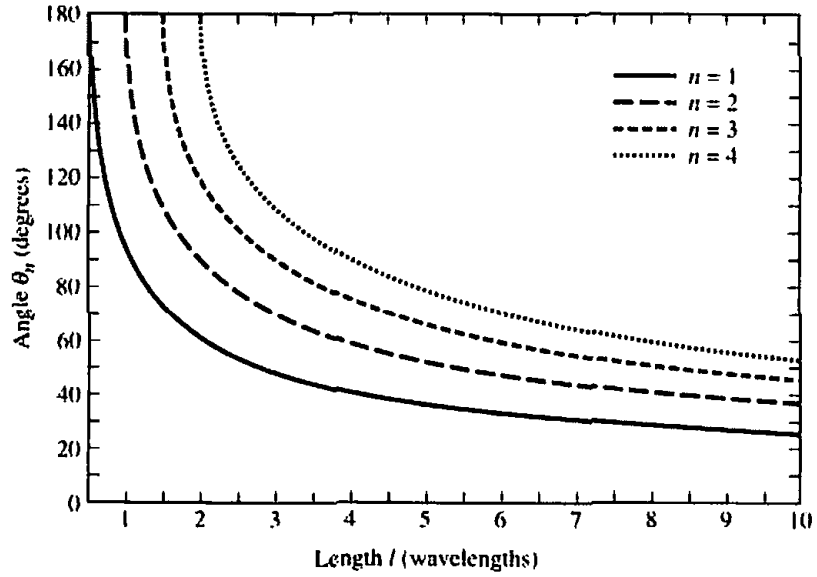


(b) Nulls

**Figure 10.7** Angles versus length of wire antenna where maxima and nulls occur.

When a TEM wave travels parallel to an air-conductor interface, it creates a forward wave tilt [2] which is determined by applying the boundary conditions on the tangential fields along the interface. The amount of tilt is a function of the constitutive parameters of the ground. If the conductor is a perfect electric conductor (PEC), then the wave tilt is zero because the tangential electric field vanishes along the PEC. The wave tilt increases with frequency and with ground resistivity. Therefore, for a Beverage wire antenna, shown in Figure 10.1(c) in the receiving mode, reception is influenced by the tilt angle of the incident vertically polarized wavefront, which is formed by the losses of the local ground. The electric field vector of the incident wavefront produces an electric force that is parallel to the wire, which in turn induces a current in the wire. The current flows in the wire toward the receiver, and it is reinforced up to a certain point along the wire by the advancing wavefront. The wave along the wire is transverse magnetic.

*D. Resonant Wires*

Resonant wire antennas are formed when the load impedance of Figure 10.1(a) is not matched to the characteristic impedance of the line. This causes reflections which with the incident wave form a standing wave. Resonant antennas, including the dipole, were examined in detail in Chapter 4, and the electric and magnetic field components of a center fed wire of total length $l$ are given, respectively, by (4-62a) and (4-62b). Other radiation characteristics (including directivity, radiation resistance, maximum effective area, etc.) are found in Chapter 4.

Resonant antennas can also be formed using long wires. It can be shown that for *resonant* long wires with lengths odd multiple of half wavelength ($l = n\lambda/2$, $n = 1, 3, 5, \ldots$), the radiation resistance is given approximately (within 0.5 ohms) by [3], [4]

$$R_r = 73 + 69 \log_{10}(n) \tag{10-16}$$

This expression gives a very good answer even for $n = 1$. For the same elements, the angle of maximum radiation is given by

$$\theta_{\max} = \cos^{-1}\left(\frac{n-1}{n}\right) \tag{10-17}$$

This formula is more accurate for small values of $n$, although it gives good results even for large values of $n$. It can also be shown that the maximum directivity is related to the radiation resistance by

$$D_0 = \frac{120}{R_r \sin^2 \theta_{\max}} \tag{10-18}$$

The values based on (10-18) are within 0.5 dB from those based on (4-75). It is apparent that all three expressions, (10-16)–(10-18), lead to very good results for the half-wavelength dipole ($n = 1$).

Long wire antennas (both resonant and nonresonant) are very simple, economical, and effective directional antennas with many uses for transmitting and receiving waves in the MF (300 KHz–3 MHz) and HF (3–30 MHz) ranges. Their properties can be enhanced when used in arrays.

## 10.2.2 V Antenna

For some applications a single long wire antenna is not very practical because (1) its directivity may be low, (2) its side lobes may be high, and (3) its main beam is inclined at an angle, which is controlled by its length. These and other drawbacks of single long wire antennas can be overcome by utilizing an array of wires.

One very practical array of long wires is the V antenna formed by using two wires each with one of its ends connected to a feed line as shown in Figure 10.8(a). In most applications, the plane formed by the legs of the V is parallel to the ground leading to a horizontal V array whose principal polarization is parallel to the ground and the plane of the V. Because of increased sidelobes, the directivity of ordinary linear dipoles begins to diminish for lengths greater than about $1.25\lambda$, as shown in Figure 4.8. However by adjusting the included angle of a V dipole, its directivity can be made greater and its side lobes smaller than those of a corresponding linear dipole. Designs for maximum directivity usually require smaller included angles for longer V's.

Most V antennas are symmetrical ($\theta_1 = \theta_2 = \theta_0$ and $l_1 = l_2 = l$). Also V antennas can be designed to have unidirectional or bidirectional radiation patterns, as

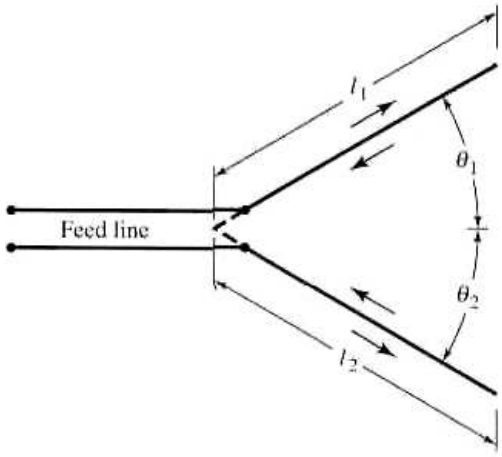


(a) V antenna

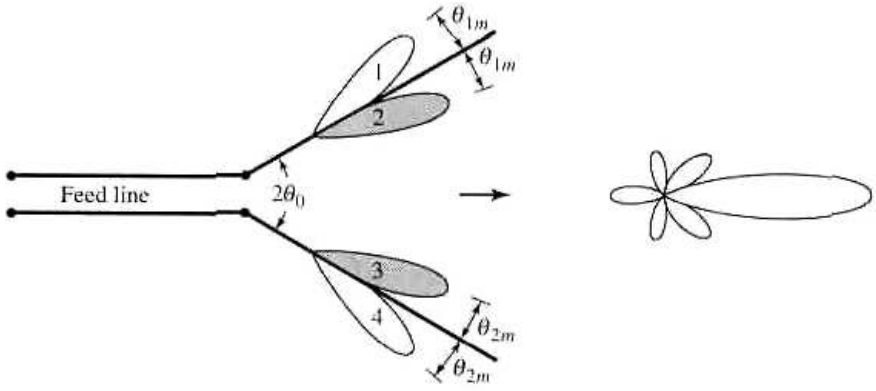


(b) Unidirectional

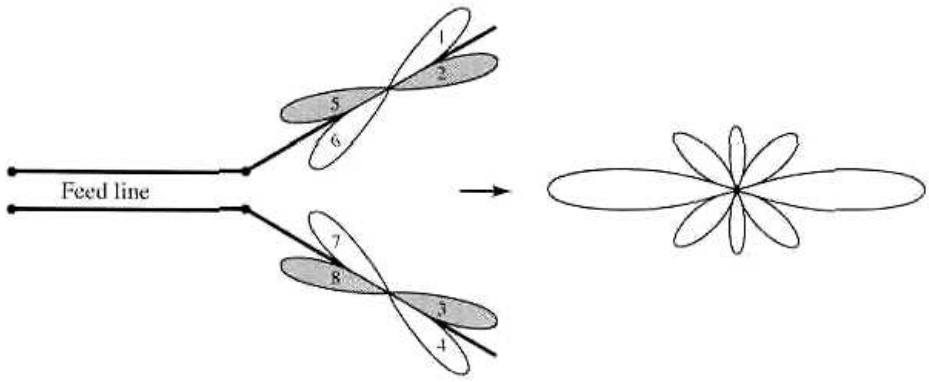


(c) Bidirectional

**Figure 10.8** Unidirectional and bidirectional V antennas.

shown in Figures 10.8(b) and (c), respectively. To achieve the unidirectional characteristics, the wires of the V antenna must be nonresonant which can be accomplished by minimizing if not completely eliminating reflections from the ends of the wire. The reflected waves can be reduced by making the inclined wires of the V relatively thick. In theory, the reflections can even be eliminated by properly terminating the open ends of the V leading to a purely traveling wave antenna. One way of terminating the V antenna will be to attach a load, usually a resistor equal in value to the open-end characteristic impedance of the V-wire transmission line, as shown in Figure

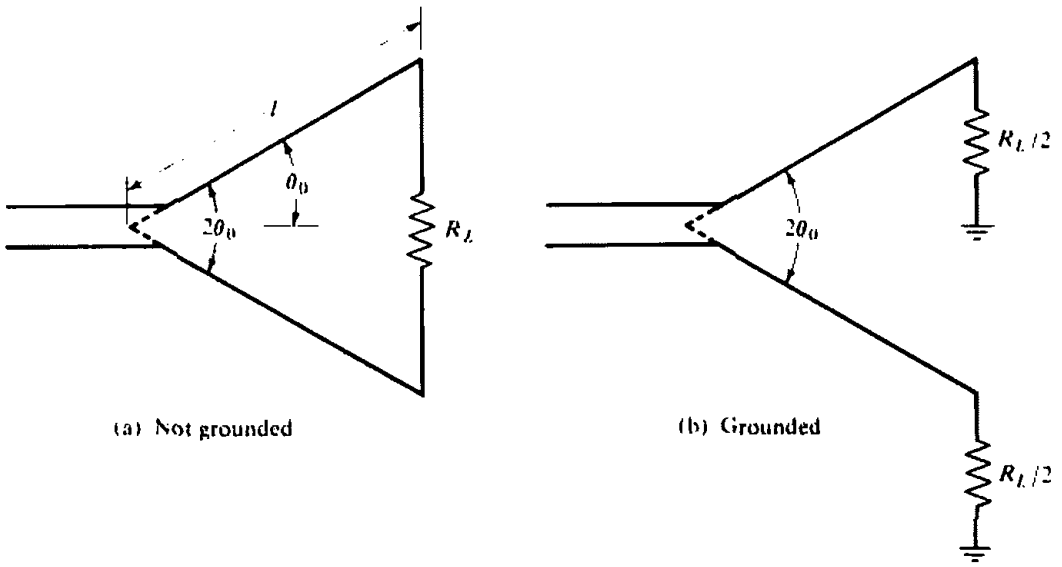


Figure 10.9 Terminated V antennas.

10.9(a). The terminating resistance can also be divided in half and each half connected to the ground leading to the termination of Figure 10.9(b). If the length of each leg of the V is very long (typically $l > 5\lambda$), there will be sufficient leakage of the field along each leg that when the wave reaches the end of the V it will be sufficiently reduced that there will not necessarily be a need for a termination. Of course, termination with a load is not possible without a ground plane.

The patterns of the individual wires of the V antenna are conical in form and are inclined at an angle from their corresponding axes. The angle of inclination is determined by the length of each wire. For the patterns of each leg of a symmetrical V antenna to add in the direction of the line bisecting the angle of the V and to form one major lobe, the total included angle $2\theta_0$ of the V should be equal to $2\theta_m$, which is twice the angle that the cone of maximum radiation of each wire makes with its axis. When this is done, beams 2 and 3 of Figure 10.8(b) are aligned and add constructively. Similarly for Figure 10.8(c), beams 2 and 3 are aligned and add constructively in the forward direction, while beams 5 and 6 are aligned and add constructively in the backward direction. If the total included angle of the V is greater than $2\theta_m$ ($2\theta_0 > 2\theta_m$) the main lobe is split into two distinct beams. However, if $2\theta_0 < 2\theta_m$, then the maximum of the single major lobe is still along the plane that bisects the V but it is tilted upward from the plane of the V. This may be a desired designed characteristic when the antenna is required to transmit waves upward toward the ionosphere for optimum reflection or to receive signals reflected downward by the ionosphere. For optimum operation, typically the included angle is chosen to be approximately $\theta_0 \approx 0.8\theta_m$. When this is done, the reinforcement of the fields from the two legs of the V lead to a total directivity for the V of approximately twice the directivity of one leg of the V.

For a symmetrical V antenna with legs each of length $l$, there is an optimum included angle which leads to the largest directivity. Design data for optimum included angles of V dipoles were computed [5] using Moment Method techniques and are shown in Figure 10.10(a). The corresponding directivities are shown in Figure 10.10(b). In each figure the dots (·) represent values computed using the Moment Method while the solid curves represent second- or third-order polynomials fitted

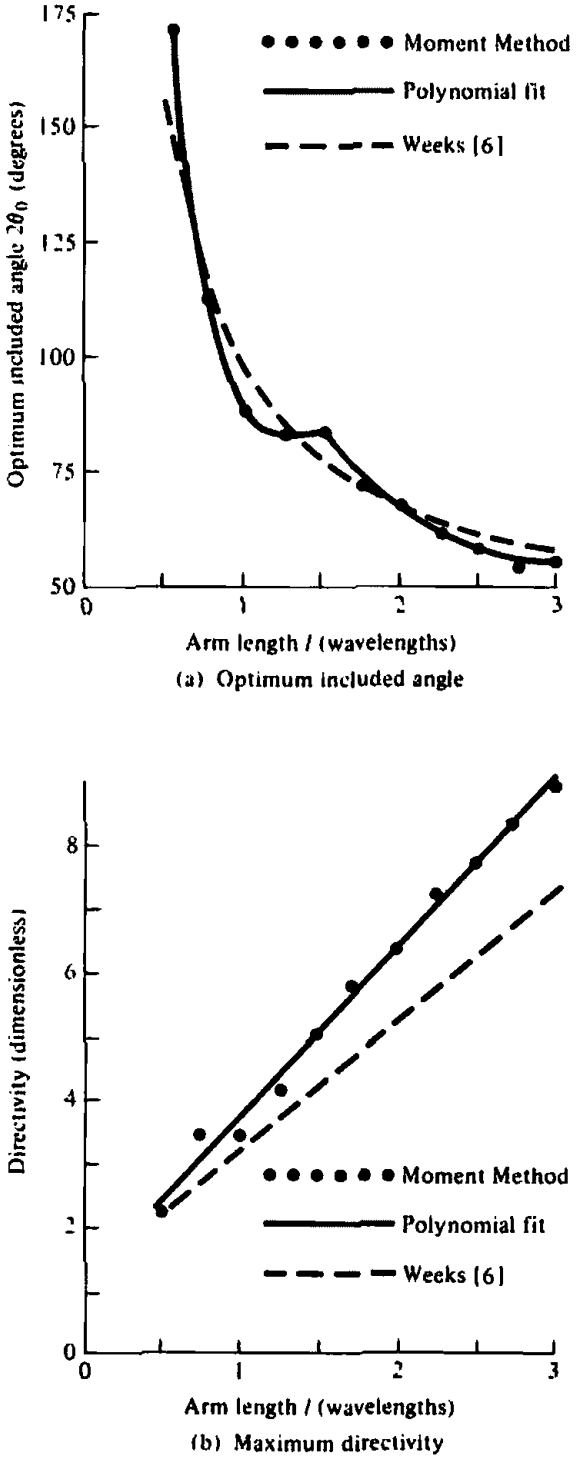


**Figure 10.10** Optimum included angle for maximum directivity as a function of arm length for V dipoles. (SOURCE: G. A. Thiele and E. P. Ekelman, Jr., "Design Formulas for Vee Dipoles," *IEEE Trans. Antennas Propagat.*, Vol. AP-28, pp. 588–590, July 1980. © (1980) IEEE)

through the computed data. The polynomials for optimum included angles and maximum directivities are given by

$$2\theta_0 = \begin{cases} -149.3\left(\frac{l}{\lambda}\right)^3 + 603.4\left(\frac{l}{\lambda}\right)^2 - 809.5\left(\frac{l}{\lambda}\right) + 443.6 & \text{for } 0.5 \le l/\lambda \le 1.5 \quad \text{(10-19a)} \\ 13.39\left(\frac{l}{\lambda}\right)^2 - 78.27\left(\frac{l}{\lambda}\right) + 169.77 & \text{for } 1.5 \le l/\lambda \le 3 \quad \text{(10-19b)} \end{cases}$$

$$D_0 = 2.94\left(\frac{l}{\lambda}\right) + 1.15 \qquad \text{for } 0.5 \le l/\lambda \le 3 \qquad \text{(10-20)}$$

The dashed curves represent data obtained from empirical formulas [6]. The corresponding input impedances of the V's are slightly smaller than those of straight dipoles.

Another form of a V antenna is shown in the insert of Figure 10.11(a). The V is formed by a monopole wire, bent at an angle over a ground plane, and by its image shown dashed. The included angle of the V as well as the length can be used to tune the antenna. For included angles greater than 120° ($2\theta_0 > 120°$), the antenna exhibits primarily vertical polarization with radiation patterns almost identical to those of straight dipoles. As the included angle becomes smaller than about 120°, a horizontally polarized field component is excited which tends to fill the pattern toward the horizontal direction, making it a very attractive communication antenna for aircraft. The computed impedance of the ground plane and free-space V configurations obtained by the Moment Method [7] is shown plotted in Figure 10.11(a).

Another practical form of a dipole antenna, particularly useful for airplane or ground-plane applications, is the 90° bent wire configuration of Figure 10.11(b). The computed impedance of the antenna, obtained also by the Moment Method [7], is shown plotted in Figure 10.11(b). This antenna can be tuned by adjusting its perpendicular and parallel lengths $h_1$ and $h_2$. The radiation pattern in the plane of the antenna is nearly omnidirectional for $h_1 \le 0.1\lambda$. For $h_1 > 0.1\lambda$ the pattern approaches that of vertical $\lambda/2$ dipole.

### 10.2.3 Rhombic Antenna

*A. Geometry and Radiation Characteristics*

Two V antennas can be connected at their open ends to form a diamond or rhombic antenna, as shown in Figure 10.12(a). The antenna is usually terminated at one end in a resistor, usually about 600–800 ohms, in order to reduce if not eliminate reflections. However, if each leg is long enough (typically greater than $5\lambda$) sufficient leakage occurs along each leg that the wave that reaches the far end of the rhombus is sufficiently reduced that it may not be necessary to terminate the rhombus. To achieve the single main lobe, beams 2, 3, 6, and 7 are aligned and add constructively. The other end is used to feed the antenna. Another configuration of a rhombus is that of Figure 9.12(b) which is formed by an inverted V and its image (shown dashed). The inverted V is connected to the ground through a resistor. As with the V antennas, the pattern of rhombic antennas can be controlled by varying the element lengths, angles

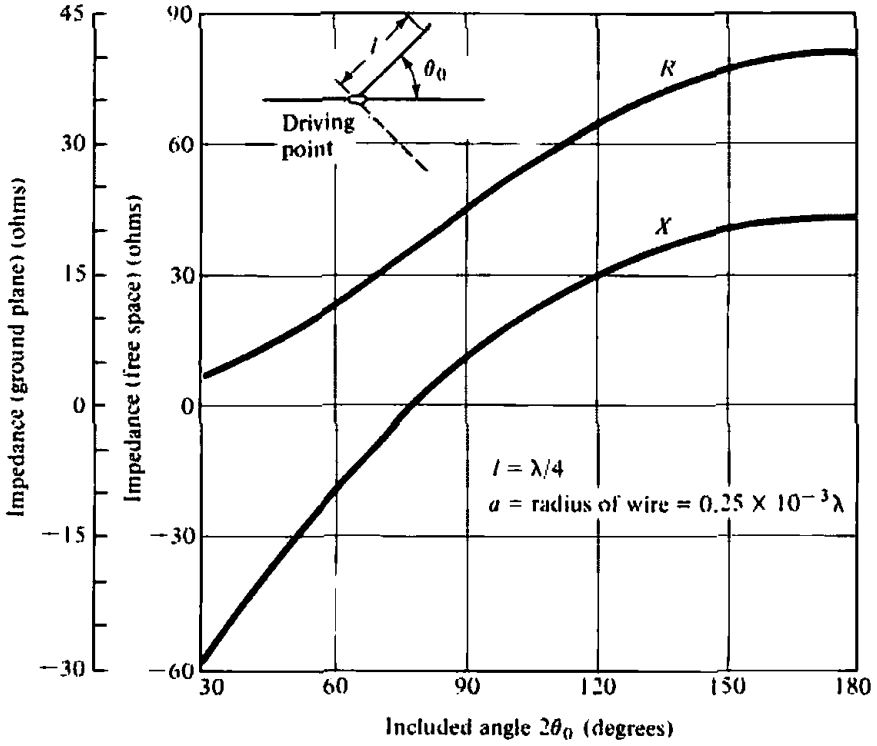


(a) V antenna

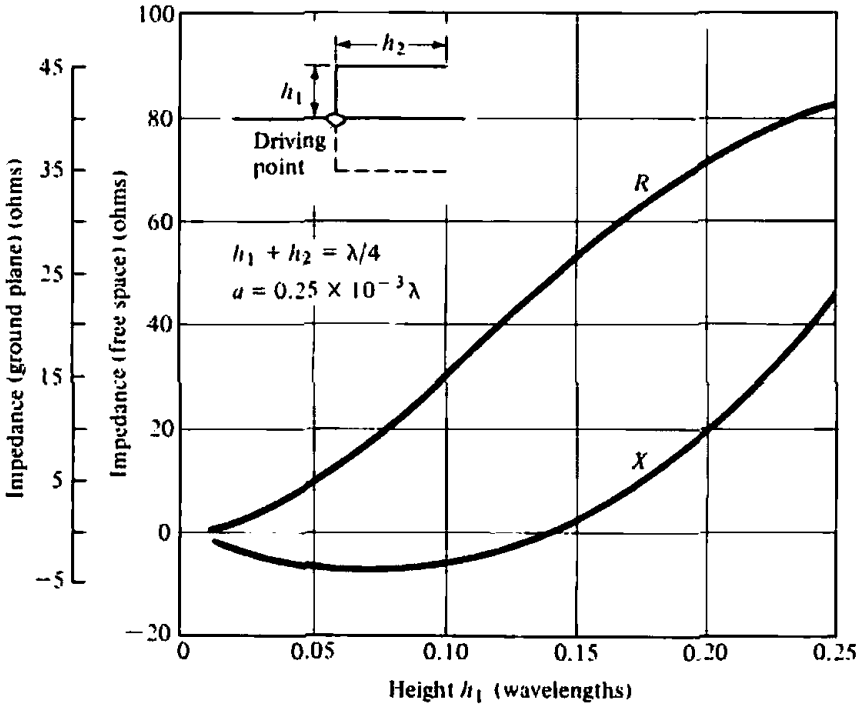


(b) Bent wire

**Figure 10.11** Computed impedance ($R + jX$) of V and bent wire antennas above ground. (SOURCE: D. G. Fink (ed.), *Electronics Engineer's Handbook*, Chapter 18 (by W. F. Croswell), McGraw-Hill, New York, 1975)

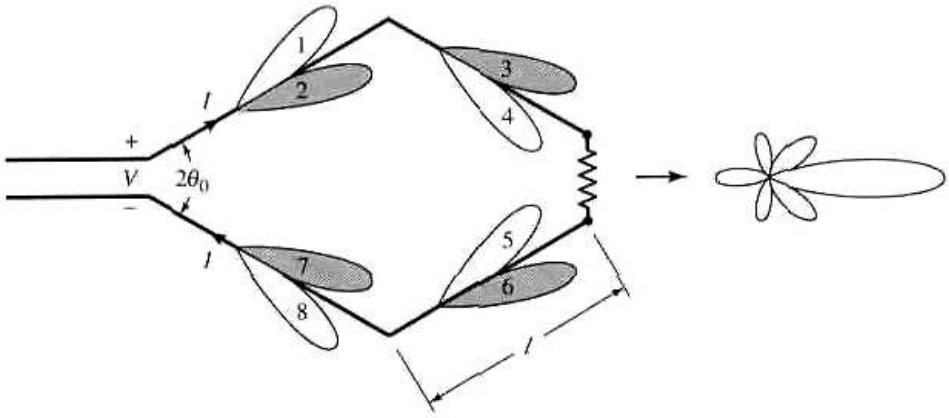


(a) Rhombus formed by 2 V's

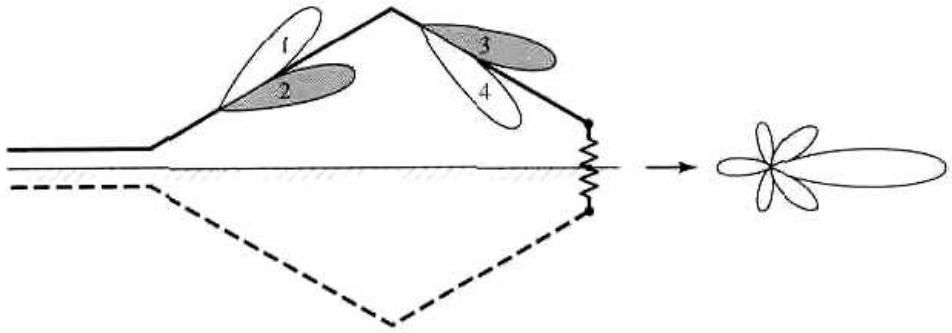


(b) Rhombus formed by inverted V over ground

**Figure 10.12** Rhombic antenna configurations.

between elements, and the plane of the rhombus. Rhombic antennas are usually preferred over V's for nonresonant and unidirectional pattern applications because they are less difficult to terminate. Additional directivity and reduction in side lobes can be obtained by stacking, vertically or horizontally, a number of rhombic and/or V antennas to form arrays.

The field radiated by a rhombus can be found by adding the fields radiated by its four legs. For a symmetrical rhombus with equal legs, this can be accomplished using array theory and pattern multiplication. When this is done, a number of design equations can be derived [8]–[11]. For this design, the plane formed by the rhombus is placed parallel and a height $h$ above a perfect electric conductor.

*B. Design Equations*

Let us assume that it is desired to design a rhombus such that the maximum of the main lobe of the pattern, in a plane which bisects the $V$ of the rhombus, is directed at an angle $\psi_0$ above the ground plane. The design can be optimized if the height $h$ is selected according to

$$\frac{h_m}{\lambda_0} = \frac{m}{4\cos(90^\circ - \psi_0)}, \qquad m = 1, 3, 5, \ldots \tag{10-21}$$

with $m = 1$ representing the minimum height.

The minimum optimum length of each leg of a symmetrical rhombus must be selected according to

$$\frac{l}{\lambda_0} = \frac{0.371}{1 - \sin(90° - \psi_0)\cos\theta_0} \tag{10-22}$$

The best choice for the included angle of the rhombus is selected to satisfy

$$\theta_0 = \cos^{-1}[\sin(90° - \psi_0)] \tag{10-23}$$

## 10.3 BROADBAND ANTENNAS

In Chapter 9 broadband dipole antennas were discussed. There are numerous other antenna designs that exhibit greater broadband characteristics than those of the dipoles. Some of these antenna can also provide circular polarization, a desired extra feature for many applications. In this section we want to discuss briefly some of the most popular broadband antennas.

### 10.3.1 Helical Antenna

Another basic, simple, and practical configuration of an electromagnetic radiator is that of a conducting wire wound in the form of a screw thread forming a helix, as shown in Figure 10.13. In most cases the helix is used with a ground plane. The ground plane can take different forms. One is for the ground to be flat, as shown in Figure 10.13. Typically the diameter of the ground plane should be at least $3\lambda/4$. However, the ground plane can also be cupped in the form of a cylindrical cavity or in the form of a frustrum cavity [8]. In addition, the helix is usually connected to the center conductor of a coaxial transmission line at the feed point with the outer conductor of the line attached to the ground plane.

The geometrical configuration of a helix consists usually of $N$ turns, diameter $D$ and spacing $S$ between each turn. The total length of the antenna is $L = NS$ while the total length of the wire is $L_n = NL_0 = N\sqrt{S^2 + C^2}$ where $L_0 = \sqrt{S^2 + C^2}$ is the length of the wire between each turn and $C = \pi D$ is the circumference of the helix. Another important parameter is the pitch angle $\alpha$ which is the angle formed by a line tangent to the helix wire and a plane perpendicular to the helix axis. The pitch angle is defined by

$$\boxed{\alpha = \tan^{-1}\left(\frac{S}{\pi D}\right) = \tan^{-1}\left(\frac{S}{C}\right)} \tag{10-24}$$

When $\alpha = 0°$, then the winding is flattened and the helix reduces to a loop antenna of $N$ turns. On the other hand, when $\alpha = 90°$ then the helix reduces to a linear wire. When $0° < \alpha < 90°$, then a true helix is formed with a circumference greater than zero but less than the circumference when the helix is reduced to a loop ($\alpha = 0°$).

The radiation characteristics of the antenna can be varied by controlling the size of its geometrical properties compared to the wavelength. The input impedance is critically dependent upon the pitch angle and the size of the conducting wire, especially near the feed point, and it can be adjusted by controlling their values. The general polarization of the antenna is elliptical. However circular and linear polarizations can be achieved over different frequency ranges.

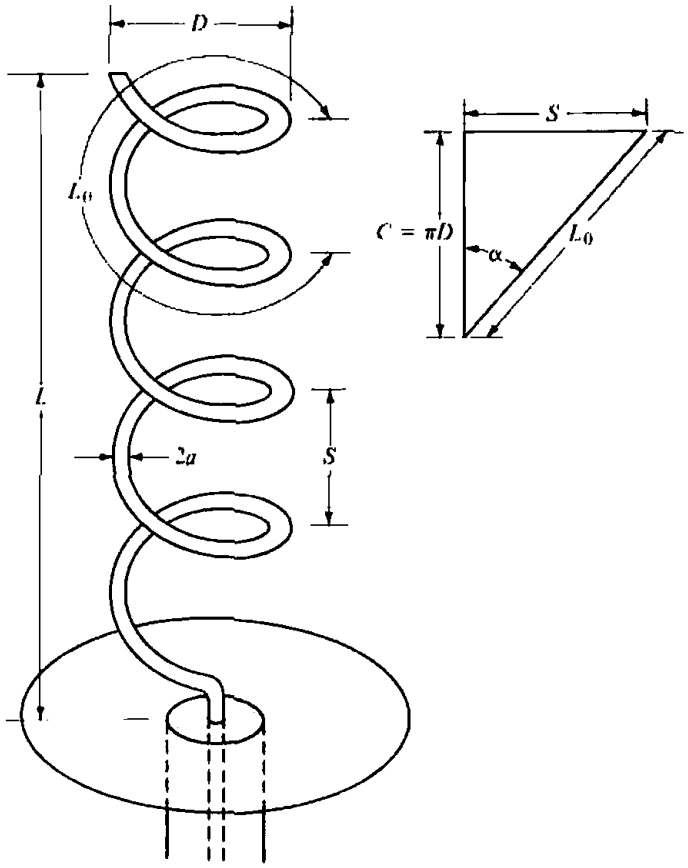


**Figure 10.13** Helical antenna with ground plane.

The helical antenna can operate in many modes; however the two principal ones are the normal (broadside) and the axial (endfire) modes. The axial (endfire) mode is usually the most practical because it can achieve circular polarization over a wider bandwidth (usually 2:1) and it is more efficient.

Because an elliptically polarized antenna can be represented as the sum of two orthogonal linear components in time-phase quadrature, a helix can always receive a signal transmitted from a rotating linearly polarized antenna. Therefore helices are usually positioned on the ground for space telemetry applications of satellites, space probes, and ballistic missiles to transmit or receive signals that have undergone Faraday rotation by traveling through the ionosphere.

*A. Normal Mode*

In the normal mode of operation the field radiated by the antenna is maximum in a plane normal to the helix axis and minimum along its axis, as shown sketched in Figure 10.14(a), which is a figure-eight rotated about its axis similar to that of a linear dipole of $l < \lambda$ or a small loop ($a \ll \lambda$). To achieve the normal mode of operation, the dimensions of the helix are usually small compared to the wavelength (i.e., $NL_0 \ll \lambda$).

The geometry of the helix reduces to a loop of diameter $D$ when the pitch angle approaches zero and to a linear wire of length $S$ when it approaches 90°. Since the limiting geometries of the helix are a loop and a dipole, the far-field radiated by a small helix in the normal mode can be described in terms of $E_\theta$ and $E_\phi$ components of the dipole and loop, respectively. In the normal mode, it can be thought that the helix consists of $N$ small loops and $N$ short dipoles connected together in series as

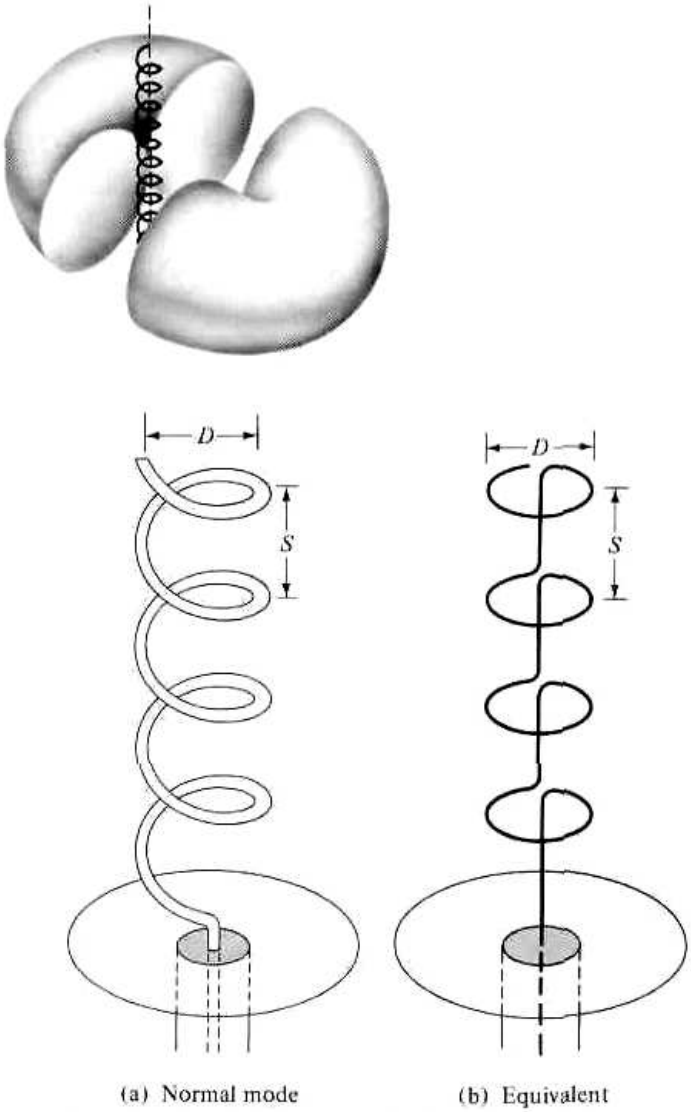


**Figure 10.14** Normal (broadside) mode for helical antenna and its equivalent.

shown in Figure 10.14(b). The fields are obtained by superposition of the fields from these elemental radiators. The planes of the loops are parallel to each other and perpendicular to the axes of the vertical dipoles. The axes of the loops and dipoles coincide with the axis of the helix.

Since in the normal mode the helix dimensions are small, the current throughout its length can be assumed to be constant and its relative far-field pattern to be independent of the number of loops and short dipoles. Thus its operation can be described accurately by the sum of the fields radiated by a small loop of radius $D$ and a short dipole of length $S$, with its axis perpendicular to the plane of the loop, and each with the same constant current distribution.

The far-zone electric field radiated by a short dipole of length $S$ and constant current $I_0$ is $E_\theta$, and it is given by (4-26a) as

$$E_\theta = j\eta \frac{kI_0 Se^{-jkr}}{4\pi r} \sin\theta \tag{10-25}$$

where $l$ is being replaced by $S$. In addition the electric field radiated by a loop is $E_\phi$, and it is given by (5-27b) as

$$E_\phi = \eta \frac{k^2(D/2)^2 I_0 e^{-jkr}}{4r} \sin\theta \tag{10-26}$$

where $D/2$ is substituted for $a$. A comparison of (10-25) and (10-26) indicates that *the two components are in time-phase quadrature, a necessary but not sufficient* condition for circular or elliptical polarization.

The ratio of the magnitudes of the $E_\theta$ and $E_\phi$ components is defined as the axial ratio (AR), and it is given by

$$\boxed{\text{AR} = \frac{|E_\theta|}{|E_\phi|} = \frac{4S}{\pi k D^2} = \frac{2\lambda S}{(\pi D)^2}} \tag{10-27}$$

By varying the $D$ and/or $S$ the axial ratio attains values of $0 \le \text{AR} \le \infty$. The value of AR = 0 is a special case and occurs when $E_\theta = 0$ leading to a linearly polarized wave of horizontal polarization (the helix is a loop). When AR = $\infty$, $E_\phi = 0$ and the radiated wave is linearly polarized with vertical polarization (the helix is a vertical dipole). Another special case is the one when AR is unity (AR = 1) and occurs when

$$\frac{2\lambda S}{(\pi D)^2} = 1 \tag{10-28}$$

or

$$\boxed{C = \pi D = \sqrt{2S\lambda}} \tag{10-28a}$$

for which

$$\boxed{\tan\alpha = \frac{S}{\pi D} = \frac{\pi D}{2\lambda}} \tag{10-29}$$

When the dimensional parameters of the helix satisfy the above relation, the radiated field is circularly polarized in *all directions* other than $\theta = 0°$ where the fields vanish.

When the dimensions of the helix do not satisfy any of the above special cases, the field radiated by the antenna is not circularly polarized. The progression of polarization change can be described geometrically by beginning with the pitch angle of zero degrees ($\alpha = 0°$), which reduces the helix to a loop with linear horizontal polarization. As $\alpha$ increases, the polarization becomes ellipitical with the major axis being horizontally polarized. When $\alpha$, is such that $C/\lambda = \sqrt{2S/\lambda}$, AR = 1 and we have circular polarization. For greater values of $\alpha$, the polarization again becomes elliptical but with the major axis vertically polarized. Finally when $\alpha = 90°$ the helix reduces to a linearly polarized vertical dipole.

To achieve the normal mode of operation, it has been assumed that the current throughout the length of the helix is of constant magnitude and phase. This is satisfied to a large extent provided the total length of the helix wire $NL_0$ is very small compared to the wavelength ($L_n \ll \lambda$) and its end is terminated properly to reduce multiple reflections. Because of the critical dependence of its radiation characteristics on its geometrical dimensions, which must be very small compared to the wavelength, this mode of operation is very narrow in bandwidth and its radiation efficiency is very small. Practically this mode of operation is limited, and it is seldom utilized.

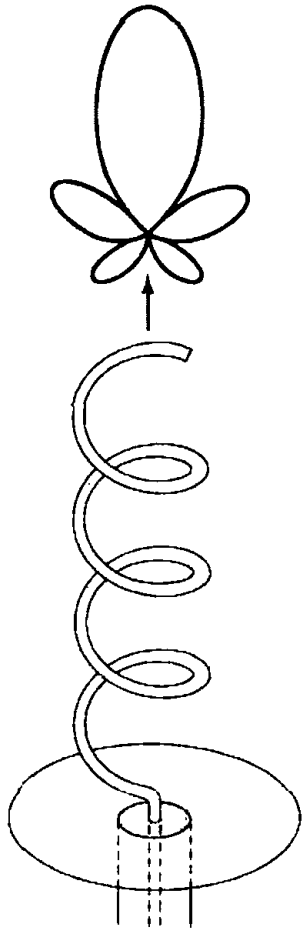

Figure 10.15 Axial (endfire) mode of helix.

*B. Axial Mode*

A more practical mode of operation, which can be generated with great ease, is the axial or endfire mode. In this mode of operation, there is only one major lobe and its maximum radiation intensity is along the axis of the helix, as shown in Figure 10.15. The minor lobes are at oblique angles to the axis.

To excite this mode, the diameter $D$ and spacing $S$ must be large fractions of the wavelength. To achieve circular polarization, primarily in the major lobe, the circumference of the helix must be in the $\frac{3}{4} < C/\lambda < \frac{4}{3}$ range (with $C/\lambda = 1$ near optimum), and the spacing about $S \simeq \lambda/4$. The pitch angle is usually $12° \leq \alpha \leq 14°$. Most often the antenna is used in conjunction with a ground plane, whose diameter is at least $\lambda/2$, and it is fed by a coaxial line. However other types of feeds (such as waveguides and dielectric rods) are possible, especially at microwave frequencies. The dimensions of the helix for this mode of operation are not as critical, thus resulting in a greater bandwidth.

*C. Design Procedure*

The terminal impedance of a helix radiating in the axial mode is nearly resistive with values between 100 and 200 ohms. Smaller values, even near 50 ohms, can be obtained by properly designing the feed. Empirical expressions, based on a large number of measurements, have been derived [8] and they are used to determine a number of parameters. The input impedance (purely resistive) is obtained by

$$R \simeq 140\left(\frac{C}{\lambda}\right) \tag{10-30}$$

which is accurate to about $\pm 20\%$, the half-power beamwidth by

$$\text{HPBW (degrees)} \simeq \frac{52\lambda^{3/2}}{C\sqrt{NS}} \tag{10-31}$$

the beamwidth between nulls by

$$\text{FNBW (degrees)} \simeq \frac{115\lambda^{3/2}}{C\sqrt{NS}} \tag{10-32}$$

the directivity by

$$D_0 \text{ (dimensionless)} \simeq 15N\frac{C^2S}{\lambda^3} \tag{10-33}$$

the axial ratio (for the condition of increased directivity) by

$$\text{AR} = \frac{2N + 1}{2N} \tag{10-34}$$

and the normalized far-field pattern by

$$E = \sin\left(\frac{\pi}{2N}\right)\cos\theta\frac{\sin[(N/2)\psi]}{\sin[\psi/2]} \tag{10-35}$$

where

$$\psi = k_0\left(S\cos\theta - \frac{L_0}{p}\right) \tag{10-35a}$$

$$p = \frac{L_0/\lambda_0}{S/\lambda_0 + 1} \qquad \text{For ordinary end-fire radiation} \tag{10-35b}$$

$$p = \frac{L_0/\lambda_0}{S/\lambda_0 + \left(\dfrac{2N + 1}{2N}\right)} \qquad \text{For Hansen-Woodyard end-fire radiation} \tag{10-35c}$$

All these relations are approximately valid provided $12° < \alpha < 14°$, $\frac{3}{4} < C/\lambda < \frac{4}{3}$, and $N > 3$.

The far-field pattern of the helix, as given by (10-35), has been developed by assuming that the helix consists of an array of $N$ identical turns (each of nonuniform current and identical to that of the others), a uniform spacing $S$ between them, and the elements are placed along the $z$-axis. The cos $\theta$ term in (10-35) represents the field pattern of a single turn, and the last term in (10-35) is the array factor of a uniform array of $N$ elements. The total field is obtained by multiplying the field from one turn with the array factor (pattern multiplication).

The value of $p$ in (10-35a) is the ratio of the wave velocity along the helix wire to that in free space, and it is selected according to (10-35b) for ordinary end-fire radiation or (10-35c) for Hansen-Woodyard end-fire radiation. These are derived as follows.

For ordinary end-fire the relative phase $\psi$ among the various turns of the helix (elements of the array) is given by (6-7a), or

$$\psi = k_0 S \cos\theta + \beta \tag{10-36}$$

where $d = S$ is the spacing between the turns of the helix. For an end-fire design, the radiation from each one of the turns along $\theta = 0°$ must be in-phase. Since the wave along the helix wire between turns travels a distance $L_0$ with a wave velocity $v = pv_0$ ($p > 1$ where $v_0$ is the wave velocity in free space) and the desired maximum radiation is along $\theta = 0°$, then (10-36) for *ordinary end-fire* radiation is equal to

$$\psi = (k_0 S \cos\theta - kL_0)_{\theta=0°} = k_0\left(S - \frac{L_0}{p}\right) = -2\pi m, \quad m = 0, 1, 2, \ldots \tag{10-37}$$

Solving (10-37) for $p$ leads to

$$p = \frac{L_0/\lambda_0}{S/\lambda_0 + m} \tag{10-38}$$

For $m = 0$ and $p = 1$, $L_0 = S$. This corresponds to a straight wire ($\alpha = 90°$), and not a helix. Therefore the next value is $m = 1$, and it corresponds to the first transmission mode for a helix. Substituting $m = 1$ in (10-38) leads to

$$p = \frac{L_0/\lambda_0}{S/\lambda_0 + 1} \tag{10-38a}$$

which is that of (10-35b).

In a similar manner, it can be shown that for Hansen-Woodyard end-fire radiation (10-37) is equal to

$$\psi = (k_0 S \cos\theta - kL_0)_{\theta=0°} = k_0\left(S - \frac{L_0}{p}\right) = -\left(2\pi m + \frac{\pi}{N}\right), \quad m = 0, 1, 2, \ldots \tag{10-39}$$

which when solved for $p$ leads to

$$p = \frac{L_0/\lambda_0}{S/\lambda_0 + \left(\dfrac{2mN + 1}{2N}\right)} \tag{10-40}$$

For $m = 1$, (10-40) reduces to

$$p = \frac{L_0/\lambda_0}{S/\lambda_0 + \left(\dfrac{2N + 1}{2N}\right)} \tag{10-40a}$$

which is identical to (10-35c).

*D. Feed Design*

The nominal impedance of a helical antenna operating in the axial mode, computed using (10-30), is 100–200 ohms. However, many practical transmission lines (such

as a coax) have characteristic impedance of about 50 ohms. In order to provide a better match, the input impedance of the helix must be reduced to near that value. There may be a number of ways by which this can be accomplished. One way to effectively control the input impedance of the helix is to properly design the first 1/4 turn of the helix which is next to the feed [8], [12]. To bring the input impedance of the helix from nearly 150 ohms down to 50 ohms, the wire of the first 1/4 turn should be flat in the form of a strip and the transition into a helix should be very gradual. This is accomplished by making the wire from the feed, at the beginning of the formation of the helix, in the form of a strip of width $w$ by flattening it and nearly touching the ground plane which is covered with a dielectric slab of height [2]

$$h = \frac{w}{\frac{377}{\sqrt{\epsilon_r}\, Z_0} - 2} \tag{10-41}$$

where

$w$ = width of strip conductor of the helix starting at the feed

$\epsilon_r$ = dielectric constant of the dielectric slab covering the ground plane

$Z_0$ = characteristic impedance of the input transmission line

Typically the strip configuration of the helix transitions from the strip to the regular circular wire and the designed pitch angle of the helix very gradually within the first 1/4–1/2 turn.

This modification decreases the characteristic impedance of the conductor-ground plane effective transmission line, and it provides a lower impedance over a substantial but reduced bandwidth. For example, a 50-ohm helix has a VSWR of less than 2:1 over a 40% bandwidth compared to a 70% bandwidth for a 140-ohm helix. In addition, the 50-ohm helix has a VSWR of less than 1.2:1 over a 12% bandwidth as contrasted to a 20% bandwidth for one of 140 ohms.

A simple and effective way of increasing the thickness of the conductor near the feed point will be to bond a thin metal strip to the helix conductor [12]. For example, a metal strip 70-mm wide was used to provide a 50-ohm impedance in a helix whose conducting wire was 13-mm in diameter and it was operating at 230.77 MHz.

### 10.3.2 Electric-Magnetic Dipole

It has been shown in the previous section that the circular polarization of a helical antenna operating in the normal mode was achieved by assuming that the geometry of the helix is represented by a number of horizontal small loops and vertical infinitesimal dipoles. It would then seem reasonable that an antenna with only one loop and a single vertical dipole would, in theory, represent a radiator with an elliptical polarization. Ideally circular polarization, in all space, can be achieved if the current in each element can be controlled, by dividing the available power equally between the dipole and the loop, so that the magnitude of the field intensity radiated by each is equal.

Experimental models of such an antenna were designed and built [13] one operating around 350 MHz and the other near 1.2 GHz. A sketch of one of them is shown in Figure 10.16. The measured VSWR in the 1.15–1.32 GHz frequency range was less than 2:1.

This type of an antenna is very useful in UHF communication networks where considerable amount of fading may exist. In such cases the fading of the horizontal

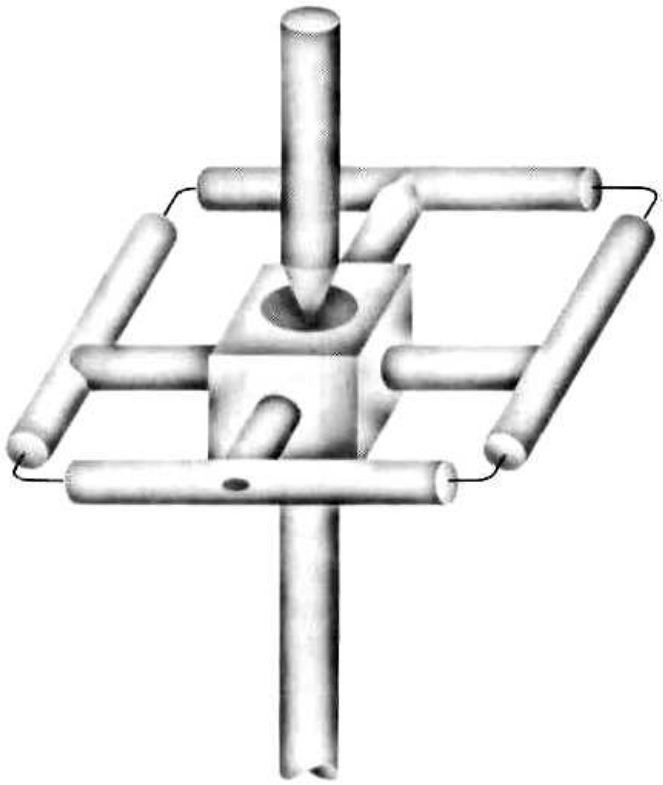

**Figure 10.16** Electric-magnetic dipole configuration. (SOURCE: A. G. Kandoian, "Three New Antenna Types and Their Applications," *Proc. IRE*, Vol. 34, pp. 70W–75W, February 1946. © (1946) IEEE)

and vertical components are affected differently and will not vary in the same manner. Hopefully, even in severe cases, there will always be one component all the time which is being affected less than the other, thus providing continuous communication. The same results would apply in VHF and/or UHF broadcasting. In addition, a transmitting antenna of this type would also provide the versatility to receive with horizontally or vertically polarized elements, providing a convenience in the architectural design of the receiving station.

### 10.3.3 Yagi-Uda Array of Linear Elements

Another very practical radiator in the HF (3–30 MHz), VHF (30–300 MHz), and UHF (300–3,000 MHz) ranges is the Yagi-Uda antenna. This antenna consists of a number of linear dipole elements, as shown in Figure 10.17, one of which is energized directly by a feed transmission line while the others act as parasitic radiators whose currents are induced by mutual coupling. The most common feed element for a Yagi-Uda antenna is a folded dipole. This radiator is exclusively designed to operate as an endfire array, and this is accomplished by having the parasitic elements in the forward beam act as directors while those in the rear act as reflectors. Yagi designated the row of directors as a "wave canal." The Yagi-Uda array is widely used as a home TV antenna; so it should be familiar to most of the readers, if not to the general public.

The original design and operating principles of this radiator were first described in Japanese in articles published in the Journal of I.E.E. of Japan by S. Uda of the Tohoku Imperial University in Japan [14]. In a later, but more widely circulated and read article [15], one of Professor Uda's colleagues H. Yagi described the operation of the same radiator in English. This paper has been considered a classic, and it was

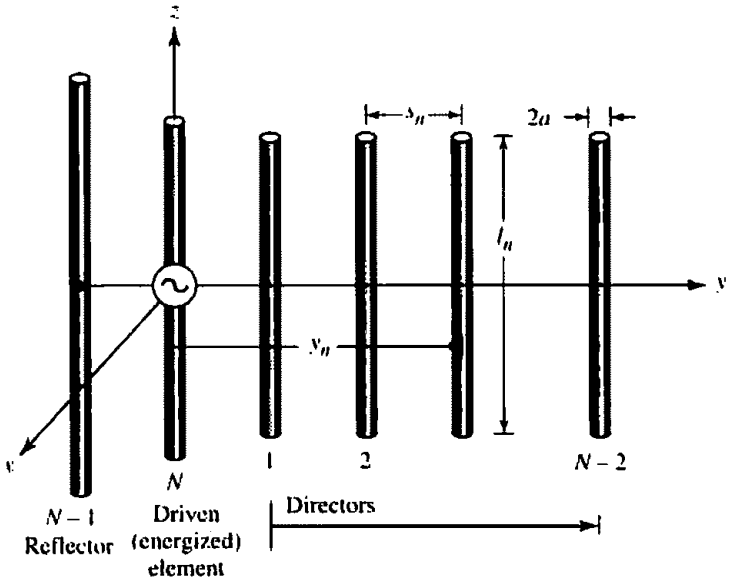


**Figure 10.17** Yagi-Uda antenna configuration.

reprinted in 1984 in its original form in the *Proceedings of the IEEE* [15] as part of IEEE's centennial celebration. Despite the fact that Yagi in his English written paper acknowledged the work of Professor Uda on beam radiators at a wavelength of 4.4 m, it became customary throughout the world to refer to this radiator as a *Yagi* antenna, a generic term in the antenna dictionary. However, in order for the name to reflect more appropriately the contributions of both inventors, it should be called a *Yagi-Uda* antenna, a name that will be adopted in this book. Although the work of Uda and Yagi was done in the early 1920s and published in the middle 1920s, full acclaim in the United States was not received until 1928 when Yagi visited the United States and presented papers at meetings of the Institute of Radio Engineers (IRE) in New York, Washington, and Hartford. In addition, his work was published in the *Proceedings of IRE*, June 1928, where J. H. Dellinger, Chief of Radio Division, Bureau of Standards, Washington, D.C., and himself a pioneer of radio waves, characterized as "exceptionally fundamental" and wrote "I have never listened to a paper that I felt so sure was destined to be a classic." So true!!

*The Yagi-Uda antenna has received exhaustive analytical and experimental investigations* in the open literature and elsewhere. It would be impractical to list all the contributors, many of whom we may not be aware. However, we will attempt to summarize the salient point of the analysis, describe the general operation of the radiator, and present some design data.

To achieve the endfire beam formation, the parasitic elements in the direction of the beam are somewhat smaller in length than the feed element. Typically the driven element is resonant with its length slightly less than $\lambda/2$ (usually $0.45$–$0.49\lambda$) whereas the lengths of the directors will be about 0.4 to $0.45\lambda$. However, the directors are not necessarily of the same length and/or diameter. The separation between the directors is typically 0.3 to $0.4\lambda$, and it is not necessarily uniform for optimum designs. It has been shown experimentally that for a Yagi-Uda array of $6\lambda$ total length the overall gain was independent of director spacing up to about $0.3\lambda$. A significant drop (5–7 dB) in gain was noted for director spacings greater than $0.3\lambda$. For that antenna, the gain was also independent of the radii of the directors up to about $0.024\lambda$. The length of

the reflector is somewhat greater than that of the feed. In addition, the separation between the driven element and the reflector is somewhat smaller than the spacing between the driven element and the nearest director, and it is found to be near optimum at $0.25\lambda$.

Since the length of each director is smaller than its corresponding resonant length, the impedance of each is capacitive and its current leads the induced emf. Similarly the impedances of the reflectors is inductive and the phases of the currents lag those of the induced emfs. The total phase of the currents in the directors and reflectors is not determined solely by their lengths but also by their spacing to the adjacent elements. Thus, properly spaced elements with lengths slightly less than their corresponding resonant lengths (less than $\lambda/2$) act as directors because they form an array with currents approximately equal in magnitude and with equal progressive phase shifts which will reinforce the field of the energized element toward the directors. Similarly, a properly spaced element with a length of $\lambda/2$ or slightly greater will act as a reflector. Thus a Yagi-Uda array may be regarded as a structure supporting a traveling wave whose performance is determined by the current distribution in each element and the phase velocity of the traveling wave. It should be noted that the previous discussion on the lengths of the directors, reflectors, and driven elements is based on the first resonance. Higher resonances are available near lengths of $\lambda$, $3\lambda/2$, and so forth, but are seldom used.

In practice, the major role of the reflector is played by the first element next to the one energized, and very little in the performance of a Yagi-Uda antenna is gained if more than one (at the most two) elements are used as reflectors. However, considerable improvements can be achieved if more directors are added to the array. Practically there is a limit beyond which very little is gained by the addition of more directors because of the progressive reduction in magnitude of the induced currents on the more extreme elements. Usually most antennas have about 6 to 12 directors. However, many arrays have been designed and built with 30 to 40 elements. Array lengths on the order of $6\lambda$ have been mentioned [16] as typical. A gain (relative to isotropic) of about 5 to 9 per wavelength is typical for such arrays, which would make the overall gain on the order of about 30 to 54 (14.8–17.3 dB) typical.

The radiation characteristics that are usually of interest in a Yagi-Uda antenna are the *forward and backward gains, input impedance, bandwidth, front-to-back ratio,* and *magnitude of minor lobes.* The lengths and diameters of the directors and reflectors, as well as their respective spacings, determine the optimum characteritics. For a number of years optimum designs were accomplished experimentally. However, with the advent of high-speed computers many different numerical techniques, based on analytical formulations, have been utilized to derive the geometrical dimensions of the array for optimum operational performance. Usually Yagi-Uda arrays have low input impedance and relatively narrow bandwidth (on the order of about 2%). Improvements in both can be achieved at the expense of others (such as gain, magnitude of minor lobes, etc.). Usually a compromise is made, and it depends on the particular design. One way to increase the input impedance without affecting the performance of other parameters is to use an impedance step-up element as a feed (such as a two-element folded dipole with a step-up ratio of about 4). Front-to-back ratios of about 30 ($\simeq$15 dB) can be achieved at wider than optimum element spacings, but they usually are compromised somewhat to improve other desirable characteristics. For optimum designs, the minor lobes are about 30% or less ($-5.23$ dB or smaller) of the maximum.

The Yagi-Uda array can be summarized by saying that its performance can be considered in three parts:

1. the reflector-feeder arrangement
2. the feeder
3. the rows of directors

It has been concluded, numerically and experimentally, that the reflector spacing and size have (1) negligible effects on the forward gain and (2) large effects on the backward gain (front-to-back ratio) and input impedance, and they can be used to control or optimize antenna parameters without affecting the gain significantly. The feeder length and radius has a small effect on the forward gain but a large effect on the backward gain and input impedance. Its geometry is usually chosen to control the input impedance that most commonly is made real (resonant element). The size and spacing of the directors have a large effect on the forward gain, backward gain, and input impedance, and they are considered to be the most critical elements of the array.

Yagi-Uda arrays are quite common in practice because they are lightweight, simple to build, low cost, and provide moderately desirable characteristics (including a unidirectional beam) for many applications. The design for a small number of elements (typically five or six) is simple but the design becomes quite critical if a large number of elements are used to achieve a high directivity. To increase the directivity of a Yagi-Uda array or to reduce the beamwidth in the $E$-plane, several rows of Yagi-Uda arrays can be used [17] to form a curtain antenna. To neutralize the effects of the feed transmission line, an odd number of rows is usually used.

*A. Theory: Integral Equation-Moment Method*

There have been many experimental [18], [19] investigations and analytical [20]–[29] formulations of the Yagi-Uda array. A method [24] based on rigorous integral equations for the electric field radiated by the elements in the array will be presented and it will be used to describe the complex current distributions on all the elements, the phase velocity, and the corresponding radiation patterns. The method is similar to that of [24], which is based on Pocklington's integral equation of (8-24) while the one presented here follows that of [24] but is based on Pocklington's integral equation of (8-22) and formulated by Tirkas [25]. Mutual interactions are also included and, in principle, there are no restrictions on the number of elements. However, for computational purposes, point-matching numerical methods, based on the techniques of Section 8.4, are used to evaluate and satisfy the integral equation at discrete points on the axis of each element rather than everywhere on the surface of every element. The number of discrete points where boundary conditions are matched must be sufficient in number to allow the computed data to compare well with experimental results.

The theory is based on Pocklington's integral equation of (8-22) for the total field generated by an electric current source radiating in an unbounded free space, or

$$\int_{-l/2}^{+l/2} I(z')\left(\frac{\partial^2}{\partial z^2} + k^2\right)\frac{e^{-jkR}}{R}\,dz' = j4\pi\omega\epsilon_0 E_z^i \tag{10-42}$$

where

$$R = \sqrt{(x - x')^2 + (y - y')^2 + (z - z')^2} \tag{10-42a}$$

Since

$$\frac{\partial^2}{\partial z^2}\left(\frac{e^{-jkR}}{R}\right) = \frac{\partial^2}{\partial z'^2}\left(\frac{e^{-jkR}}{R}\right) \tag{10-43}$$

(10-42) reduces to

$$\int_{-l/2}^{+l/2} I(z')\frac{\partial^2}{\partial z'^2}\left(\frac{e^{-jkR}}{R}\right)dz' + k^2\int_{-l/2}^{+l/2} I(z')\frac{e^{-jkR}}{R}dz' = j4\pi\omega\epsilon_0 E_z^t \tag{10-44}$$

We will now concentrate in the integration of the first term of (10-44). Integrating the first term of (10-44) by parts where

$$u = I(z') \tag{10-45}$$

$$du = \frac{dI(z')}{dz'}dz' \tag{10-45a}$$

$$dv = \frac{\partial^2}{\partial z'^2}\left(\frac{e^{-jkR}}{R}\right)dz' = \frac{\partial}{\partial z'}\left[\frac{\partial}{\partial z'}\left(\frac{e^{-jkR}}{R}\right)\right]dz' \tag{10-46}$$

$$v = \frac{\partial}{\partial z'}\left(\frac{e^{-jkR}}{R}\right) \tag{10-46a}$$

reduces it to

$$\int_{-l/2}^{+l/2} I(z')\frac{\partial^2}{\partial z'^2}\left(\frac{e^{-jkR}}{R}\right)dz' = I(z')\left[\frac{\partial}{\partial z'}\left(\frac{e^{-jkR}}{R}\right)\right]\Bigg|_{-l/2}^{+l/2} - \int_{-l/2}^{+l/2}\frac{\partial}{\partial z'}\left(\frac{e^{-jkR}}{R}\right)\frac{dI(z')}{dz'}dz' \tag{10-47}$$

Since we require that the current at the ends of each wire vanish [i.e., $I_z(z' = +l/2) = I_z(z' = -l/2) = 0$], (10-47) reduces to

$$\int_{-l/2}^{+l/2} I(z')\frac{\partial^2}{\partial z'^2}\left(\frac{e^{-jkR}}{R}\right)dz' = -\int_{-l/2}^{+l/2}\frac{\partial}{\partial z'}\left(\frac{e^{-jkR}}{R}\right)dz'\frac{dI(z')}{dz'} \tag{10-48}$$

Integrating (10-48) by parts where

$$u = \frac{dI(z')}{dz'} \tag{10-49}$$

$$du = \frac{d^2I(z')}{dz'^2}dz' \tag{10-49a}$$

$$dv = \frac{\partial}{\partial z'}\left(\frac{e^{-jkR}}{R}\right)dz' \tag{10-50}$$

$$v = \frac{e^{-jkR}}{R} \tag{10-50a}$$

reduces (10-48) to

$$\int_{-l/2}^{+l/2} I(z')\frac{\partial^2}{\partial z'^2}\left(\frac{e^{-jkR}}{R}\right)dz' = -\frac{dI(z')}{dz'}\frac{e^{-jkR}}{R}\bigg|_{-l/2}^{+l/2} + \int_{-l/2}^{+l/2}\frac{d^2I(z')}{dz'^2}\frac{e^{-jkR}}{R}\,dz' \tag{10-51}$$

When (10-51) is substituted for the first term of (10-44) reduces (10-44) to

$$-\frac{dI(z')}{dz'}\frac{e^{-jkR}}{R}\bigg|_{l/2}^{-l/2} + \int_{-l/2}^{+l/2}\left[k^2I(z') + \frac{d^2I(z')}{dz'^2}\right]\frac{e^{-jkR}}{R}\,dz' = j4\pi\omega\epsilon_0 E_z^i \tag{10-52}$$

For small diameter wires the current on each element can be approximated by a finite series of odd-ordered even modes. Thus, the current on the $n$th element can be written as a Fourier series expansion of the form [26]

$$I_n(z') = \sum_{m=1}^{M} I_{nm}\cos\left[(2m-1)\frac{\pi z'}{l_n}\right] \tag{10-53}$$

where $I_{nm}$ represents the complex current coefficient of mode $m$ on element $n$ and $l_n$ represents the corresponding length of the $n$ element. Taking the first and second derivatives of (10-53) and substituting them, along with (10-53), into (10-52) reduces it to

$$\sum_{m=1}^{M} I_{nm}\left\{\frac{(2m-1)\pi}{l_n}\sin\left[(2m-1)\frac{\pi z_n'}{l_n}\right]\frac{e^{-jkR}}{R}\bigg|_{-l_n/2}^{+l_n/2} + \left[k^2 - \frac{(2m-1)^2\pi^2}{l_n^2}\right] \times \int_{-l_n/2}^{+l_n/2}\cos\left[(2m-1)\frac{\pi z_n'}{l_n}\right]\frac{e^{-jkR}}{R}\,dz_n'\right\} = j4\pi\omega\epsilon_0 E_z^i \tag{10-54}$$

Since the cosine is an even function, (10-54) can be reduced by integrating over only $0 \le z' \le l/2$ to

$$\sum_{m=1}^{M} I_{nm}\left\{(-1)^{m+1}\frac{(2m-1)\pi}{l_n}G_2\left(x, x', y, y'/z, \frac{l_n}{2}\right) + \left[k^2 - \frac{(2m-1)^2\pi^2}{l_n^2}\right] \times \int_0^{l_n/2} G_2(x, x', y, y'/z, z_n')\cos\left[\frac{(2m-1)\pi z_n'}{l_n}\right]dz_n'\right\} = j4\pi\omega\epsilon_0 E_z^i \tag{10-55}$$

where

$$G_2(x, x', y, y'/z, z_n') = \frac{e^{-jkR_-}}{R_-} + \frac{e^{-jkR_+}}{R_+} \tag{10-55a}$$

$$R_\pm = \sqrt{(x-x')^2 + (y-y')^2 + a^2 + (z \pm z')^2} \tag{10-55b}$$

$n = 1, 2, 3, \ldots, N$
$N =$ total number of elements

where

$R_\pm$ is the distance from the center of each wire radius to the center of any other wire, as shown in Figure 10.18(a).

The integral equation of (10-55) is valid for each element, and it assumes that the

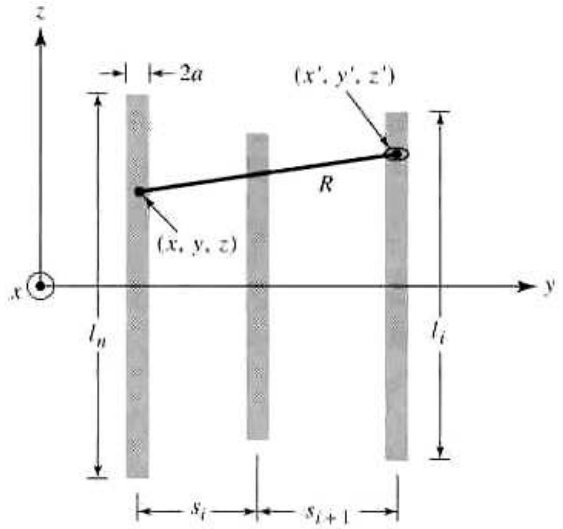


(a) Separation distance

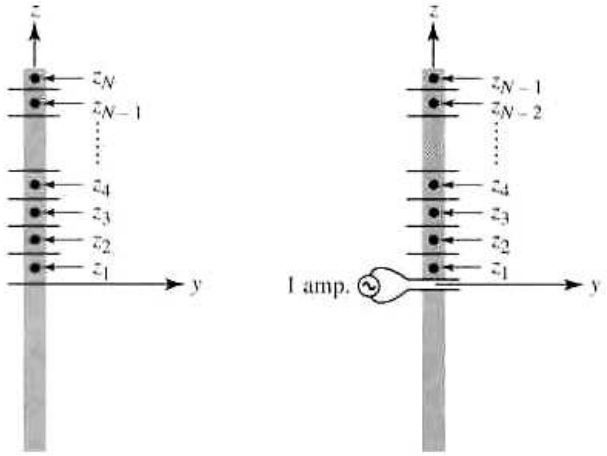


(b) Parasitic elements (c) Driven element

**Figure 10.18** Geometry of Yagi–Uda array for Moment Method formulation (SOURCE: G. A. Thiele, "Yagi-Uda Type Antennas," *IEEE Trans. Antennas Propagat.*, Vol. AP-17, No. 1, pp. 24–31, January 1969. © (1969) IEEE)

number $M$ of current modes is the same for each element. To apply the Moment Method solution to the integral equation of (10-55), each wire element is subdivided in $M$ segments. On each element, other than the driven element, the matching is done at the center of the wire, and it is required that $E_z^t$ of (10-55) vanishes at each matching point of each segment [i.e., $E_z^t(z = z_i) = 0$], as shown in Figure 10.18(b). On the driven element the matching is done on the surface of the wire, and it is required that $E_z^t$ of (10-55) vanishes at $M - 1$ points, even though there are $m$ modes, and it excludes the segment at the feed as shown in Figure 10.18(c). This generates $M - 1$ equations. The $M$th equation on the feed element is generated by the constraint that the normalized current for all $M$ modes at the feed point ($z' = 0$) of the driven element is equal to unity [24], [26], or

$$\sum_{m=1}^{M} I_{nm}(z' = 0)\Big|_{n=N} = 1 \tag{10-56}$$

Based on the above procedure, a system of linear equations is generated by taking into account the interaction of

a. each mode in each wire segment with each segment on the same wire.
b. each mode in each wire segment with each segment on the other wires.

This system of linear equations is then solved to find the complex amplitude coefficients of the current distribution in each wire as represented by (10-53). This is demonstrated in [24] for a three-element array (one director, one reflector and the driven element) with two modes in each wire.

*B. Far-Field Pattern*

Once the current distribution is found, the far-zone field generated by each element can be found using the techniques outlined in Chapter 3. The total field of the entire Yagi-Uda array is obtained by summing the contributions from each.

Using the procedure outlined in Chapter 3, the far-zone electric field generated by the $M$ modes of the $n$th element oriented parallel to the $z$ axis is given by

$$E_{\theta n} \simeq -j\omega A_{\theta n} \tag{10-57}$$

$$\begin{aligned} A_{\theta n} &\simeq -\frac{\mu e^{-jkr}}{4\pi r}\sin\theta \int_{-l_n/2}^{+l_n/2} I_n e^{jk(x_n \sin\theta\cos\phi + y_n \sin\theta\sin\phi + z_n'\cos\theta)}\, dz_n' \\ &\simeq -\frac{\mu e^{-jkr}}{4\pi r}\sin\theta \left[ e^{jk(x_n \sin\theta\cos\phi + y_n \sin\theta\sin\phi)} \int_{-l_n/2}^{+l_n/2} I_n e^{jkz_n'\cos\theta}\, dz_n' \right] \end{aligned} \tag{10-57a}$$

where $x_n$, $y_n$ represent the position of the $n$th element. The total field is then obtained by summing the contributions from each of the $N$ elements, and it can be written as

$$E_\theta = \sum_{n=1}^{N} E_{\theta n} = -j\omega A_\theta \tag{10-58}$$

$$\begin{aligned} A_\theta = \sum_{n=1}^{N} A_{\theta n} = -\frac{\mu e^{-jkr}}{4\pi r}\sin\theta \sum_{n=1}^{N} \Bigg\{ & e^{jk(x_n \sin\theta\cos\phi + y_n \sin\theta\sin\phi)} \\ & \times \left[ \int_{-l_n/2}^{+l_n/2} I_n e^{jkz_n'\cos\theta}\, dz_n' \right] \Bigg\} \end{aligned} \tag{10-58a}$$

For each wire, the current is represented by (10-53). Therefore the last integral in (10-58a) can be written as

$$\int_{-l_n/2}^{+l_n/2} I_n e^{jkz_n'\cos\theta}\, dz_n' = \sum_{m=1}^{M} I_{nm} \int_{-l_n/2}^{+l_n/2} \cos\left[\frac{(2m-1)\pi z_n'}{l_n}\right] e^{jkz_n'\cos\theta}\, dz_n' \tag{10-59}$$

Since the cosine is an even function, (10-59) can also be expressed as

$$\begin{aligned} \int_{-l_n/2}^{+l_n/2} I_n e^{jkz_n'\cos\theta}\, dz_n' = \sum_{m=1}^{M} I_{nm} \int_{0}^{+l_n/2} & 2\cos\left[\frac{(2m-1)\pi z_n'}{l_n}\right] \\ & \times \left[\frac{e^{jkz_n'\cos\theta} + e^{-jkz_n'\cos\theta}}{2}\right] dz_n' \end{aligned}$$

(Equation continues on top of page 521.)

$$= \sum_{m=1}^{M} I_{nm} \int_0^{+l_n/2} 2\cos\left[\frac{(2m-1)\pi z_n'}{l_n}\right] \times \cos(kz_n' \cos\theta)\, dz_n' \tag{10-60}$$

Using the trigonometric identity

$$2\cos(\alpha)\cos(\beta) = \cos(\alpha+\beta) + \cos(\alpha-\beta) \tag{10-61}$$

(10-60) can be rewritten as

$$\int_{-l_n/2}^{+l_n/2} I_n e^{jkz_n'\cos\theta}\, dz_n' = \sum_{m=1}^{M} I_{nm} \left\{ \int_0^{+l_n/2} \cos\left[\frac{(2m-1)\pi}{l_n} + k\cos\theta\right] z_n'\, dz_n' + \int_0^{+l_n/2} \cos\left[\frac{(2m-1)\pi}{l_n} - k\cos\theta\right] z_n'\, dz_n' \right. \tag{10-62}$$

Since

$$\int_0^{a/2} \cos[(b \pm c)z]\, dz = \frac{\alpha}{2} \frac{\sin[(b \pm c)\frac{a}{2}]}{(b \pm c)\frac{a}{2}} \tag{10-63}$$

(10-62) can be reduced to

$$\int_{-l_n/2}^{+l_n/2} I_n e^{jkz_n'\cos\theta}\, dz_n' = \sum_{m=1}^{M} I_{nm} \left[\frac{\sin(Z^+)}{Z^+} + \frac{\sin(Z^-)}{Z^-}\right] \frac{l_n}{2} \tag{10-64}$$

$$Z^+ = \left[\frac{(2m-1)\pi}{l_n} + k\cos\theta\right] \frac{l_n}{2} \tag{10-64a}$$

$$Z^- = \left[\frac{(2m-1)\pi}{l_n} - k\cos\theta\right] \frac{l_n}{2} \tag{10-64b}$$

Thus, the total field represented by (10-58) and (10-58a) can be written as

$$E_\theta = \sum_{n=1}^{N} E_{\theta n} = -j\omega A \tag{10-65}$$

$$A_\theta = \sum_{n=1}^{N} A_{\theta n} = -\frac{\mu e^{-jkr}}{4\pi r} \sin\theta \sum_{n=1}^{N} \left\{ e^{jk(x_n \sin\theta\cos\phi + y_n \sin\theta\sin\phi)} \cdot \sum_{m=1}^{M} I_{nm} \left[\frac{\sin(Z^+)}{Z^+} + \frac{\sin(Z^-)}{Z^-}\right] \right\} \frac{l_n}{2} \tag{10-65a}$$

There have been other analyses [27], [28] based on the integral equation formulation that allows the conversion to algebraic equations. In order not to belabor further the analytical formulations, which in call cases are complicated because of the antenna structure, it is appropriate at this time to present some results and indicate design procedures.

*C. Computer Program and Results*

Based on the preceding formulation, a computer program has been developed [25] that computes the *E*- and *H*-plane patterns, their corresponding half-power beamwidths, and the directivity of the Yagi-Uda array. The program is included at the end of this chapter. The input parameters include the total number of elements ($N$), the

number of current modes in each element ($M$), the length of each element, and the spacing between the elements. The program assumes one reflector, one driven element, and $N - 2$ directors. For the development of the formulation and computer program, the numbering system ($n = 1, 2, \ldots, N$) for the elements begins with the first director ($n = 1$), second director ($n = 2$), etc. The reflector is represented by the next to the last element ($n = N - 1$), while the driven element is designated as the last element ($n = N$), as shown in Figure 10.17.

One Yagi-Uda array design is considered here, which is the same as one of the two included in [24]; the other one is assigned as an end of the chapter problem. The patterns, beamwidths, and directivities were computed based on the computer program developed here.

---

**Example 10.1**

Design a Yagi-Uda array of 15 elements (13 directors, one reflector and the exciter). Compute and plot the $E$- and $H$-plane patterns, normalized current at the center of each element, and directivity and front-to-back ratio as a function of reflector spacing and director spacing. Use the computer program at the end of the chapter. The dimensions of the array are as follows.

$$\begin{aligned} N = \text{total number of elements} &= 15 \\ \text{number of directors} &= 13 \\ \text{number of reflectors} &= 1 \\ \text{number of exciters} &= 1 \\ \text{total length of reflector} &= 0.5\lambda \\ \text{total length of feeder} &= 0.47\lambda \\ \text{total length of each director} &= 0.406\lambda \\ \text{spacing between reflector and feeder} &= 0.25\lambda \\ \text{spacing between adjacent directors} &= 0.34\lambda \\ a = \text{radius of wires} &= 0.003\lambda \end{aligned}$$

SOLUTION

Using the computer program at the end of the chapter, the computed $E$- and $H$-plane patterns of this design are shown in Figure 10.19. The corresponding beamwidths are: $E$-plane ($\Theta_e = 26.98°$), $H$-plane ($\Theta_h = 27.96°$) while the directivity is 14.64 dB. A plot of the current at the center of each element versus position of the element is shown in Figure 10.20; the current of the feed element at its center is unity, as required by (10-56). One important *figure-of-merit* in Yagi-Uda array is the *front-to-back* ratio of the pattern $[20 \log_{10} E(\theta = 90°, \phi = 90°)/E(\theta = 90°, \phi = 270°)]$ as a function of the spacing of the reflector with respect to the feeder. This, along with the directivity, is shown in Figure 10.21 for spacing from $0.1\lambda$–$0.5\lambda$. For this design, the maximum front-to-back ratio occurs for a reflector spacing of about $0.23\lambda$ while the directivity is monotonically decreasing very gradually, from about 15.2 dB at a spacing of $0.1\lambda$ down to about 10.4 dB at a spacing of $0.5\lambda$.

Another important parametric investigation is the variation of the front-to-back ratio and directivity as a function of director spacing. This is shown in Figure 10.22 for spacings from $0.1\lambda$ to $0.5\lambda$. It is apparent that the directivity exhibits a slight increase from about 12 dB at a spacing of about $0.1\lambda$ to about 15.3 dB at a spacing of about $0.45\lambda$. A steep drop in directivity occurs for spacings greater than about

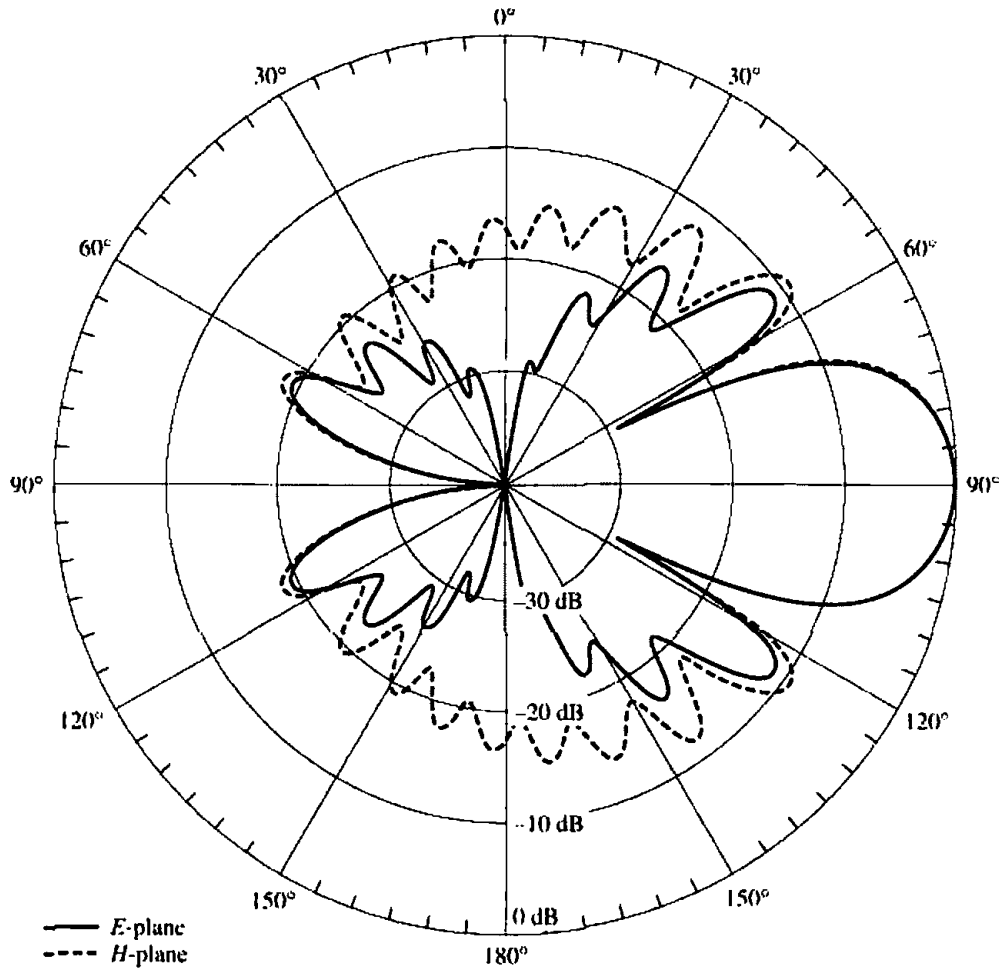


**Figure 10.19** $E$- and $H$-plane amplitude patterns of 15-element Yagi-Uda array.

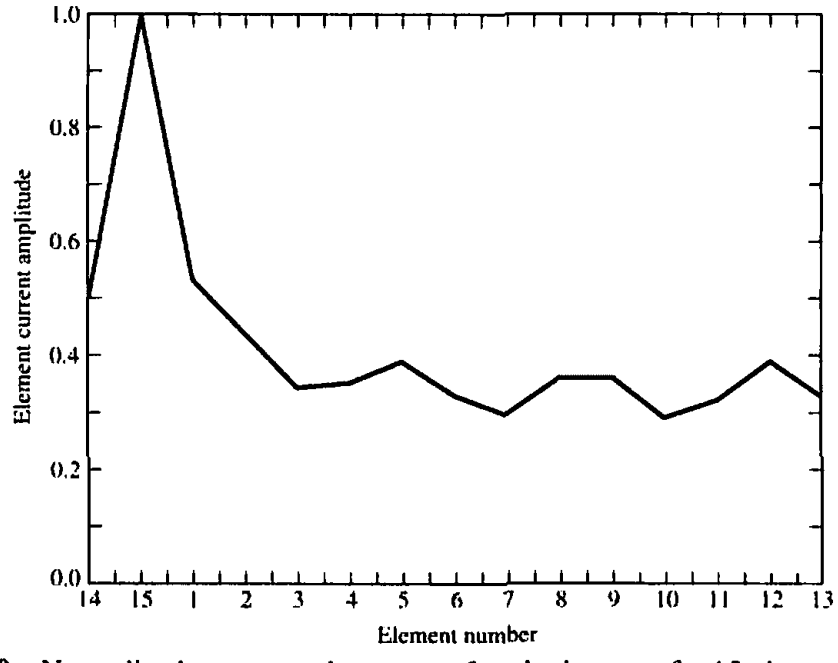


**Figure 10.20** Normalized current at the center of each element of a 15-element Yagi-Uda array.

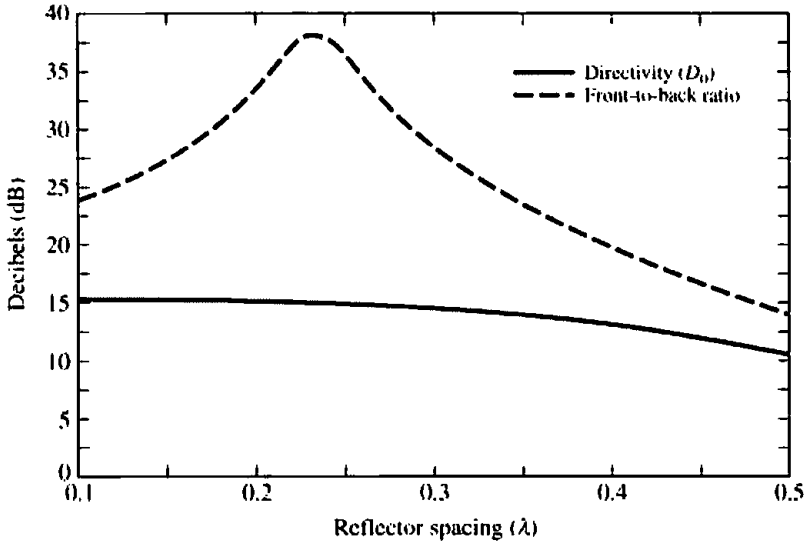


**Figure 10.21** Directivity and front-to-back ratio, as a function of reflector spacing, of a 15-element Yagi-Uda array.

0.45λ. This agrees with the conclusion arrived at in [18] and [27] that large reductions in directivity occur in Yagi-Uda array designs for spacings greater than about 0.4λ. For this design, the variations of the front-to-back ratio are much more sensitive as a function of director spacing, as shown in Figure 10.22; excursions on the order of 20–25 dB are evident for changes in spacing of about 0.05λ. Such variations in front-to-back ratio as shown in Figure 10.22, as a function of director spacing, are not evident in Yagi-Uda array designs with a smaller number of elements. However, they are even more pronounced for designs with a larger number of elements. Both of these are demonstrated in design problems assigned at the end of the chapter.

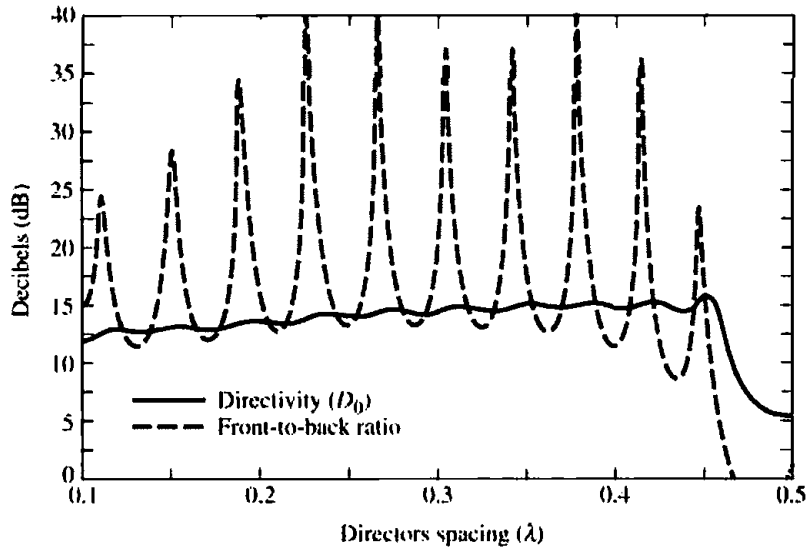


**Figure 10.22** Directivity and front-to-back ratio, as a function of director spacing, for 15-element Yagi-Uda array.

Table 10.1 DIRECTIVITY OPTIMIZATION FOR SIX-ELEMENT YAGI-UDA ARRAY (PERTURBATION OF *DIRECTOR SPACINGS*). $l_1 = 0.51\lambda$, $l_2 = 0.50\lambda$, $l_3 = l_4 = l_5 = l_6 = 0.43\lambda$, $a = 0.003369\lambda$

| | $s_{21}/\lambda$ | $s_{32}/\lambda$ | $s_{43}/\lambda$ | $s_{54}/\lambda$ | $s_{65}/\lambda$ | Directivity (dB) |
|---|---|---|---|---|---|---|
| INITIAL ARRAY | 0.250 | 0.310 | 0.310 | 0.310 | 0.310 | 11.21 |
| OPTIMIZED ARRAY | 0.250 | 0.336 | 0.398 | 0.310 | 0.407 | 12.87 |

SOURCE: D. K. Cheng and C. A. Chen, "Optimum Spacings for Yagi-Uda Arrays," *IEEE Trans. Antennas Propag.*, Vol. AP-21, pp. 615–623, September 1973. © (1973) IEEE.

*D. Optimization*

The radiation characteristics of the array can be adjusted by controlling the geometrical parameters of the array. This was demonstrated in Figures 10.21 and 10.22 for the 15-element array using uniform lengths and making uniform variations in spacings. However, these and other array characteristics can be optimized by using nonuniform director lengths and spacings between the directors. For example, the spacing between the directors can be varied while holding the reflector-exciter spacing and the lengths of all elements constant. Such a procedure was used by Cheng and Chen [27] to optimize the directivity of a six-element (four-director, reflector, exciter) array using a perturbational technique. The results of the initial and the optimized (perturbed) array are shown in Table 10.1. For the same array, they allowed all the spacings to vary while maintaining constant all other parameters. The results are shown in Table 10.2.

Another optimization procedure is to maintain the spacings between all the elements constant and vary the lengths so as to optimize the directivity. The results of a six-element array [28] are shown in Table 10.3. The ultimate optimization is to vary both the spacings and lengths. This was accomplished by Chen and Cheng [28] whereby they first optimized the array by varying the spacing, while maintaining the lengths constant. This was followed, on the same array, with perturbations in the lengths while maintaining the optimized spacings constant. The results of this procedure are shown in Table 10.4 with the corresponding $H$-plane ($\theta = \pi/2$, $\phi$) far-field patterns shown in Figure 10.23. In all, improvements in directivity and front-to-back ratio are noted. The ideal optimization will be to allow the lengths and spacings to vary simultaneously. Such an optimization was not performed in [27] or [28], although it could have been done iteratively by repeating the procedure.

Table 10.2 DIRECTIVITY OPTIMIZATION FOR SIX-ELEMENT YAGI-UDA ARRAY (PERTURBATION OF *ALL ELEMENT SPACINGS*). $l_1 = 0.51\lambda$, $l_2 = 0.50\lambda$, $l_3 = l_4 = l_5 = l_6 = 0.43\lambda$, $a = 0.003369\lambda$

| | $s_{21}/\lambda$ | $s_{32}/\lambda$ | $s_{43}/\lambda$ | $s_{54}/\lambda$ | $s_{65}/\lambda$ | Directivity (dB) |
|---|---|---|---|---|---|---|
| INITIAL ARRAY | 0.280 | 0.310 | 0.310 | 0.310 | 0.310 | 10.92 |
| OPTIMIZED ARRAY | 0.250 | 0.352 | 0.355 | 0.354 | 0.373 | 12.89 |

SOURCE: D. K. Cheng and C. A. Chen, "Optimum Spacings for Yagi-Uda Arrays," *IEEE Trans. Antennas Propag.*, Vol. AP-21, pp. 615–623, September 1973. © (1973) IEEE.

Table 10.3 DIRECTIVITY OPTIMIZATION FOR SIX-ELEMENT YAGI-UDA ARRAY (PERTURBATION OF *ALL ELEMENT LENGTHS*), $s_{21} = 0.250\lambda$, $s_{32} = s_{43} = s_{54} = s_{65} = 0.310\lambda$, $a = 0.003369\lambda$

| | $l_1/\lambda$ | $l_2/\lambda$ | $l_3/\lambda$ | $l_4/\lambda$ | $l_5/\lambda$ | $l_6/\lambda$ | Directivity (dB) |
|---|---|---|---|---|---|---|---|
| INITIAL ARRAY | 0.510 | 0.490 | 0.430 | 0.430 | 0.430 | 0.430 | 10.93 |
| LENGTH-PERTURBED ARRAY | 0.472 | 0.456 | 0.438 | 0.444 | 0.432 | 0.404 | 12.16 |

SOURCE: C. A. Chen and D. K. Cheng, "Optimum Element Lengths for Yagi-Uda Arrays," *IEEE Trans. Antennas Propag.*, Vol. AP-23, pp. 8–15, January 1975. © (1975) IEEE.

Another parameter that was investigated for the directivity-optimized Yagi-Uda antenna was the frequency bandwidth [29]. The results of such a procedure are shown in Figure 10.24. The antenna was a six-element array optimized at a center frequency $f_0$. The array was designed, using space perturbations on all the elements, to yield an optimum directivity at $f_0$. The geometrical parameters are listed in Table 10.2. The 3-dB bandwidth seems to be almost the same for the initial and the optimized arrays. The rapid decrease in the directivity of the initial and optimized arrays at frequencies higher than $f_0$ and nearly constant values below $f_0$ may be attributed to the structure of the antenna which can support a "traveling wave" at $f < f_0$ but not at $f > f_0$. It has thus been suggested that an increase in the bandwidth can be achieved if the geometrical dimensions of the antenna are chosen slightly smaller than the optimum.

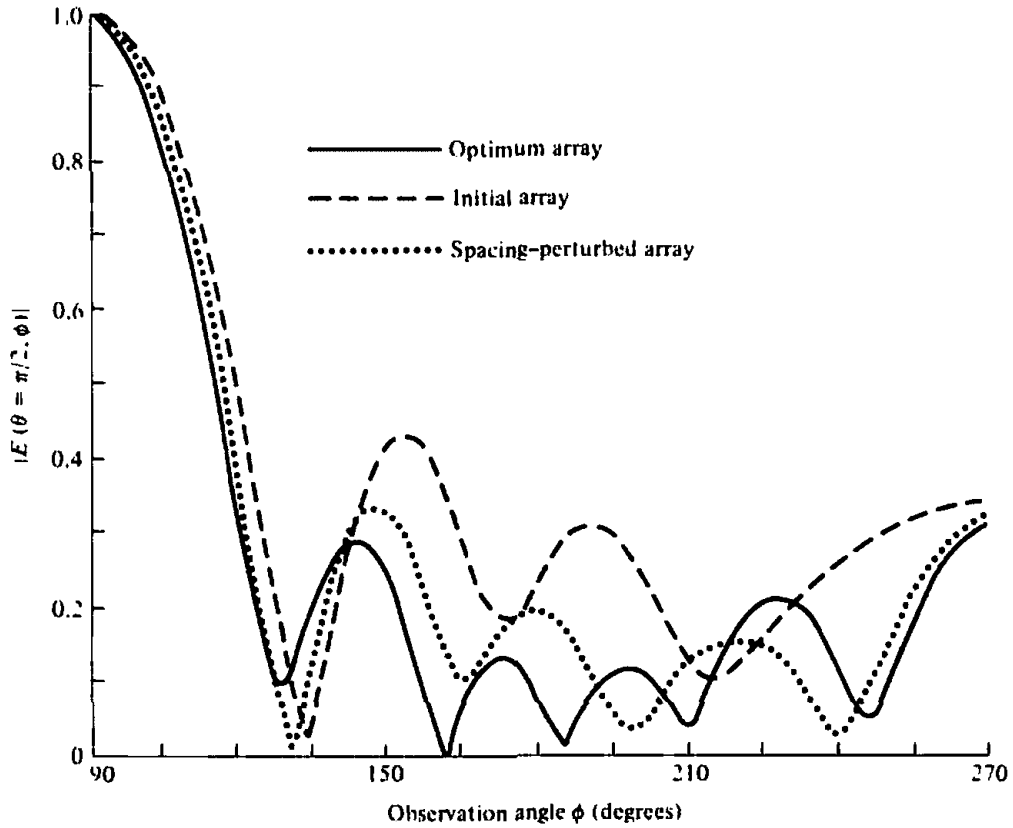


Figure 10.23 Normalized amplitude antenna patterns of initial, perturbed, and optimum six-element Yagi-Uda arrays (Table 10.4). (SOURCE: C. A. Chen and D. K. Cheng, "Optimum Element Lengths for Yagi-Uda Arrays," *IEEE Trans. Antennas Propagat.*, Vol. AP-23, pp. 8–15, January 1975. © (1975) IEEE)

**Table 10.4** DIRECTIVITY OPTIMIZATION FOR SIX-ELEMENT YAGI-UDA ARRAY (PERTURBATION OF *DIRECTOR SPACINGS AND ALL ELEMENT LENGTHS*), $a = 0.003369\lambda$

| | $l_1/\lambda$ | $l_2/\lambda$ | $l_3/\lambda$ | $l_4/\lambda$ | $l_5/\lambda$ | $l_6/\lambda$ | $s_{21}/\lambda$ | $s_{32}/\lambda$ | $s_{43}/\lambda$ | $s_{54}/\lambda$ | $s_{65}/\lambda$ | Directivity (dB) |
|---|---|---|---|---|---|---|---|---|---|---|---|---|
| INITIAL ARRAY | 0.510 | 0.490 | 0.430 | 0.430 | 0.430 | 0.430 | 0.250 | 0.310 | 0.310 | 0.310 | 0.310 | 10.93 |
| ARRAY AFTER SPACING PERTURBATION | 0.510 | 0.490 | 0.430 | 0.430 | 0.430 | 0.430 | 0.250 | 0.289 | 0.406 | 0.323 | 0.422 | 12.83 |
| OPTIMUM ARRAY AFTER SPACING AND LENGTH PERTURBATION | 0.472 | 0.452 | 0.436 | 0.430 | 0.434 | 0.430 | 0.250 | 0.289 | 0.406 | 0.323 | 0.422 | 13.41 |

SOURCE: C. A. Chen and D. K. Cheng. "Optimum Element Lengths for Yagi-Uda Arrays." *IEEE Trans. Antennas Propag.*, Vol. AP-23, pp. 8–15, January 1975. © (1975) IEEE.

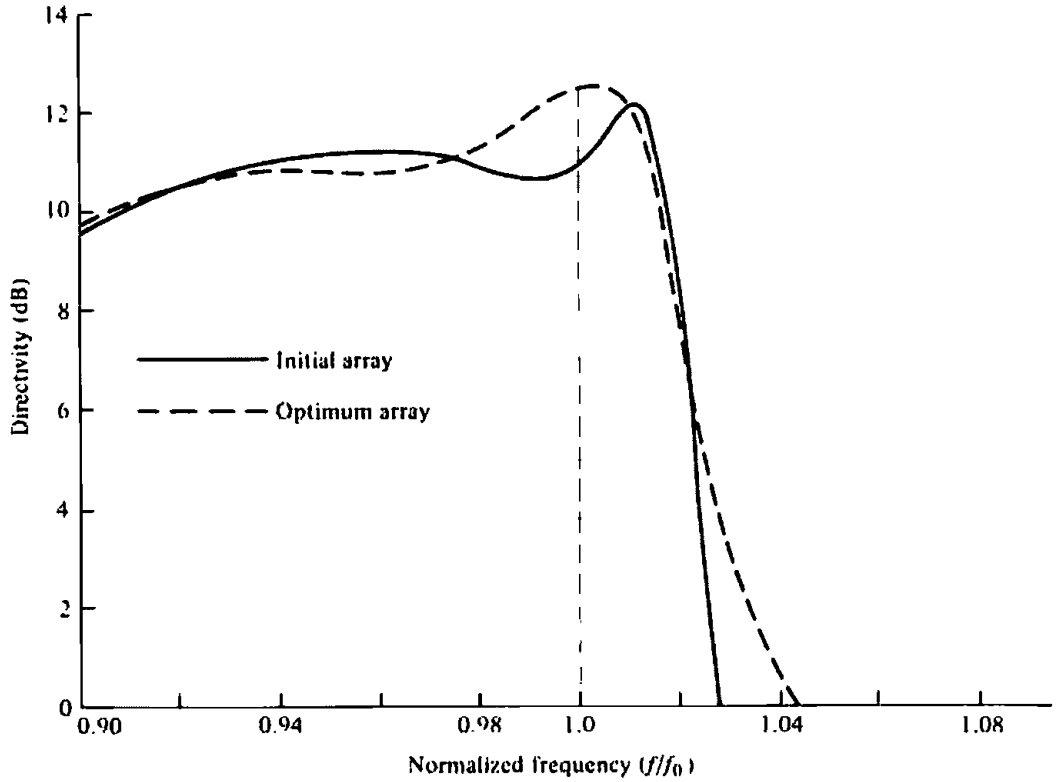


**Figure 10.24** Bandwidth of initial and optimum six-element Yagi-Uda array with perturbation of all element spacings (Table 10.2). (SOURCE: N. K. Takla and L.-C. Shen, "Bandwidth of a Yagi Array with Optimum Directivity," *IEEE Trans. Antennas Propagat.*, Vol. AP-25, pp. 913–914, November 1977. © (1977) IEEE)

*E. Input Impedance and Matching Techiques*

The input impedance of a Yagi-Uda array, measured at the center of the driven element, is usually small and it is strongly influenced by the spacing between the reflector and feed element. For a 13-element array using a resonant driven element, the measured input impedances are listed in Table 10.5 [20]. Some of these values are low for matching to a 50-, 78-, or 300-ohm transmission lines.

There are many techniques that can be used to match a Yagi-Uda array to a transmission line and eventually to the receiver, which in many cases is a television set which has a large impedance (on the order of 300 ohms). Two common matching techniques are the use of the folded dipole, of Section 9.5, as a driven element and simultaneously as an impedance transformer, and the Gamma-match of Section 9.8.4. Which one of the two is used depends primarily on the transmission line from the antenna to the receiver.

The coaxial cable is now widely used as the primary transmission line for television, especially with the wide spread and use of cable TV; in fact, most television sets are already prewired with coaxial cable connections. Therefore, if the coax with a characteristic impedance of about 78 ohms is the transmission line used from the Yagi-Uda antenna to the receiver and since the input impedance of the antenna is typically 30–70 ohms (as illustrated in Table 10.5), the Gamma-match is the most prudent matching technique to use. This has been widely used in commercial designs where a clamp is usually employed to vary the position of the short to achieve a best match.

If, however, a "twin-lead" line with a characteristic impedance of about 300 ohms is used as the transmission line from the antenna to the receiver, as was used

Table 10.5 INPUT IMPEDANCE OF A 15-ELEMENT YAGI-UDA ARRAY (REFLECTOR LENGTH = 0.5λ; DIRECTOR SPACING = 0.34λ; DIRECTOR LENGTH = 0.406λ)

| Reflector Spacing ($s_{21}/\lambda$) | Input Impedance (ohms) |
|---|---|
| 0.25 | 62 |
| 0.18 | 50 |
| 0.15 | 32 |
| 0.13 | 22 |
| 0.10 | 12 |

widely some years ago, then it would be most prudent to use a folded dipole as the driven element which acts as a step-up impedance transformer of about 4:1 (4:1 when the length of the element is exactly λ/2. This technique is also widely used in commercial designs.

Another way to explain the endfire beam formation and whether the parameters of the Yagi-Uda array are properly adjusted for optimum directivity is by drawing a vector diagram of the progressive phase delay from element-to-element. If the current amplitudes throughout the array are equal, the total phase delay for maximum directivity should be about 180°, as is required by the Hansen-Woodyard criteria for improved endfire radiation. Since the currents in a Yagi-Uda array are not equal in all the elements, the phase velocity of the traveling wave along the antenna structure is not the same from element-to-element but it is always slower than the velocity of light and faster than the corresponding velocity for a Hansen-Woodyard design. For a Yagi-Uda array, the decrease in the phase velocity is a function of the increase in total array length.

In general then, the phase velocity, and in turn the phase shift, of a traveling wave in a Yagi-Uda array structure is controlled by the geometrical dimensions of the array and its elements, and it is not uniform from element-to-element.

*F. Design Procedure*

A government document [30] has been published which provides extensive data of experimental investigations carried out by the National Bureau of Standards to determine how parasitic element diameter, element length, spacings between elements, supporting booms of different cross-sectional areas, various reflectors, and overall length affect the measured gain. Numerous graphical data is included to facilitate the design of different length antennas to yield maximum gain. In addition, design criteria are presented for stacking Yagi-Uda arrays either one above the other or side-by-side. A step-by-step design procedure has been established in determining the geometrical parameters of a Yagi-Uda array for a desired directivity (over that of a λ/2 dipole mounted at the same height above ground). The included graphs can only be used to design arrays with overall lengths (*from reflector element to last director*) of 0.4, 0.8, 1.2, 2.2, 3.2, and 4.2λ with corresponding directivities of 7.1, 9.2, 10.2, 12.25, 13.4, and 14.2 dB, respectively, and with a diameter-to-wavelength ratio of $0.001 \leq d/\lambda \leq 0.04$. Although the graphs do not cover all possible designs, they do accommodate most practical requests. The driven element used to derive the data was a λ/2 folded dipole, and the measurements were carried out at $f = 400$ MHz. To make the reader aware of the procedure, it will be outlined by the use of an example. The procedure

**Table 10.6** OPTIMIZED UNCOMPENSATED LENGTHS OF PARASITIC ELEMENTS FOR YAGI-UDA ANTENNAS OF SIX DIFFERENT LENGTHS

| $d/\lambda = 0.0085$ | | LENGTH OF YAGI-UDA (IN WAVELENGTHS) | | | | | |
|---|---|---|---|---|---|---|---|
| $s_{12} = 0.2\lambda$ | | 0.4 | 0.8 | 1.20 | 2.2 | 3.2 | 4.2 |
| LENGTH OF REFLECTOR ($l_1/\lambda$) | | 0.482 | 0.482 | 0.482 | 0.482 | 0.482 | 0.475 |
| LENGTH OF DIRECTORS, $\lambda$ | $l_3$ | 0.442 | 0.428 | 0.428 | 0.432 | 0.428 | 0.424 |
| | $l_4$ | | 0.424 | 0.420 | 0.415 | 0.420 | 0.424 |
| | $l_5$ | | 0.428 | 0.420 | 0.407 | 0.407 | 0.420 |
| | $l_6$ | | | 0.428 | 0.398 | 0.398 | 0.407 |
| | $l_7$ | | | | 0.390 | 0.394 | 0.403 |
| | $l_8$ | | | | 0.390 | 0.390 | 0.398 |
| | $l_9$ | | | | 0.390 | 0.386 | 0.394 |
| | $l_{10}$ | | | | 0.390 | 0.386 | 0.390 |
| | $l_{11}$ | | | | 0.398 | 0.386 | 0.390 |
| | $l_{12}$ | | | | 0.407 | 0.386 | 0.390 |
| | $l_{13}$ | | | | | 0.386 | 0.390 |
| | $l_{14}$ | | | | | 0.386 | 0.390 |
| | $l_{15}$ | | | | | 0.386 | 0.390 |
| | $l_{16}$ | | | | | 0.386 | |
| | $l_{17}$ | | | | | 0.386 | |
| SPACING BETWEEN DIRECTORS ($s_{ik}/\lambda$) | | 0.20 | 0.20 | 0.25 | 0.20 | 0.20 | 0.308 |
| DIRECTIVITY RELATIVE TO HALF-WAVE DIPOLE (dB) | | 7.1 | 9.2 | 10.2 | 12.25 | 13.4 | 14.2 |
| DESIGN CURVE (SEE FIGURE 10.25) | | (*A*) | (*B*) | (*B*) | (*C*) | (*B*) | (*D*) |

SOURCE: Peter P. Viezbicke. *Yagi Antenna Design*, NBS Technical Note 688, December 1976.

is identical for all other designs at freqencies where included data can accommodate the specifications.

The heart of the design is the data included in

1. Table 10.6 which represents optimized antenna parameters for six different lengths and for a $d/\lambda = 0.0085$
2. Figure 10.25 which represents *uncompensated* director and reflector lengths for $0.001 \leq d/\lambda \leq 0.04$
3. Figure 10.26 which provides compensation length increase for all the parasitic elements (directors and reflectors) as a function of boom-to-wavelength ratio $0.001 \leq D/\lambda \leq 0.04$

The specified information is usually the center frequency, antenna directivity, $d/\lambda$ and $D/\lambda$ ratios, and it is required to find the optimum parasitic element lengths (directors and reflectors). The spacing between the directors is uniform but not the same for all

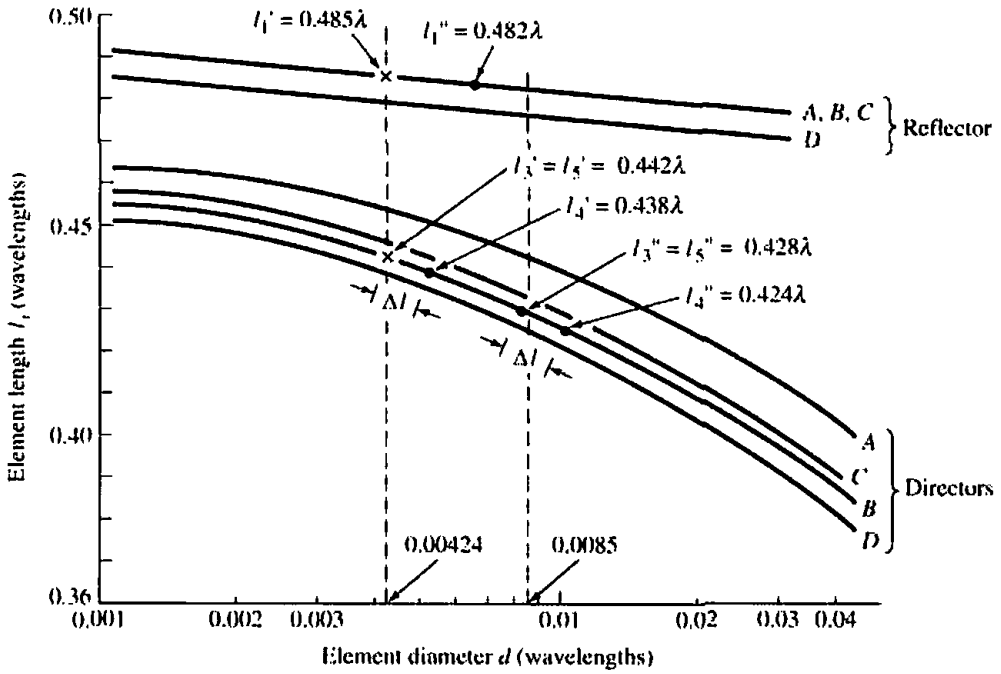


**Figure 10.25** Design curves to determine element lengths of Yagi-Uda arrays. (SOURCE: P. P. Viezbicke, "Yagi Antenna Design," NBS Technical Note 688, U.S. Department of Commerce/National Bureau of Standards, December 1976)

designs. However, there is only one reflector and its spacing is $s = 0.2\lambda$ for all designs.

---

**Example 10.2**

Design a Yagi-Uda array with a directivity (relative to a $\lambda/2$ dipole at the same height above ground) of 9.2 dB at $f_0 = 50.1$ MHz. The desired diameter of the parasitic elements is 2.54 cm and of the metal supporting boom 5.1 cm. Find the element spacings, lengths, and total array length.

SOLUTION

(a) At $f_0 = 50.1$ MHz the wavelength is $\lambda = 5.988$ m $= 598.8$ cm. Thus $d/\lambda = 2.54/598.8 = 4.24 \times 10^{-3}$ and $D/\lambda = 5.1/598.8 = 8.52 \times 10^{-3}$.

(b) From Table 10.6, the desired array would have a total of five elements (three directors, one reflector, one feeder). For a $d/\lambda = 0.0085$ ratio the optimum uncompensated lengths would be those shown in the second column of Table 10.6 ($l_3 = l_5 = 0.428\lambda$, $l_4 = 0.424\lambda$, and $l_1 = 0.482\lambda$). The overall antenna length would be $L = (0.6 + 0.2)\lambda = 0.8\lambda$, the spacing between directors $0.2\lambda$, and the reflector spacing $0.2\lambda$. It is now desired to find the optimum lengths of the parasitic elements for a $d/\lambda = 0.00424$.

(c) Plot the optimized lengths from Table 10.6 ($l_3'' = l_5'' = 0.428\lambda$, $l_4'' = 0.424\lambda$, and $l_1'' = 0.482\lambda$) on Figure 10.25 and mark them by a dot (·).

(d) In Figure 10.25 draw a vertical line through $d/\lambda = 0.00424$ intersecting curves ($B$) at director uncompensated lengths $l_3' = l_5' = 0.442\lambda$ and reflector length $l_1' = 0.485\lambda$. Mark these points by an x.

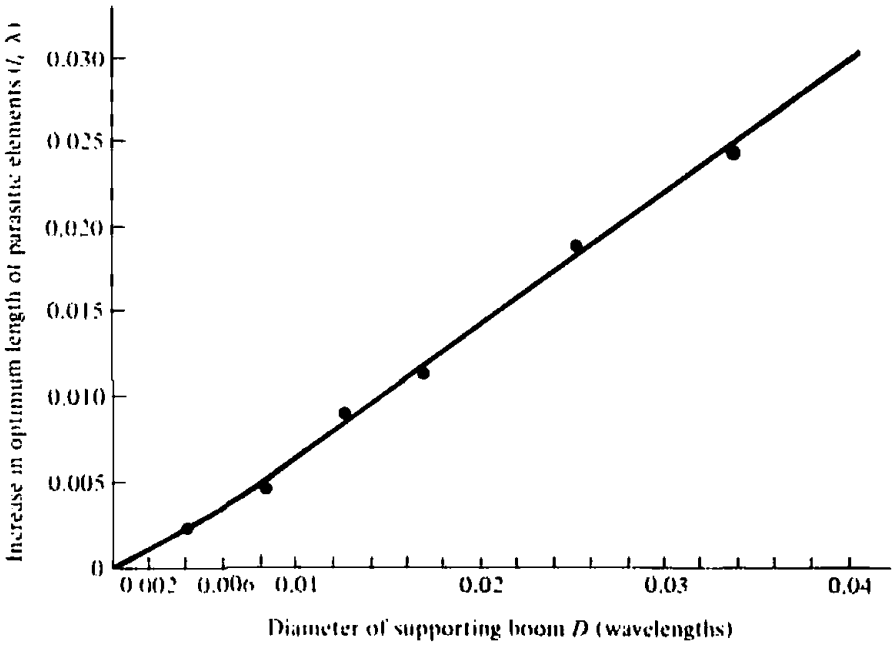


**Figure 10.26** Increase in optimum length of parasitic elements as a function of metal boom diameter. (SOURCE: P. P. Viezbicke," Yagi Antenna Design," NBS Technical Note 688, U.S. Department of Commerce/National Bureau of Standards, December 1976)

(e) With a divider, measure the distance ($\Delta l$) along director curve ($B$) between points $l_3'' = l_5'' = 0.428\lambda$ and $l_4'' = 0.424\lambda$. Transpose this distance from the point $l_3' = l_5' = 0.442\lambda$ on curve ($B$), established in step (d) and marked by an x, downward along the curve and determine the uncompensated length $l_4' = 0.438\lambda$. Thus the boom uncompensated lengths of the array at $f_0 = 50.1$ MHz are

$$l_3' = l_5' = 0.442\lambda$$
$$l_4' = 0.438\lambda$$
$$l_1' = 0.485\lambda$$

(f) Correct the element lengths to compensate for the boom diameter. From Figure 10.26, a boom diameter-to-wavelength ratio of 0.00852 requires a fractional length increase in each element of about $0.005\lambda$. Thus the final lengths of the elements should be

$$l_3 = l_5 = (0.442 + 0.005)\lambda = 0.447\lambda$$
$$l_4 = (0.438 + 0.005)\lambda = 0.443\lambda$$
$$l_1 = (0.485 + 0.005)\lambda = 0.490\lambda$$

---

The design data were derived from measurements carried out on a nonconducting Plexiglas boom mounted $3\lambda$ above the ground. The driven element was a $\lambda/2$ folded dipole matched to a 50-ohm line by a double-stub tuner. All parasitic elements were constructed from aluminum tubing. Using Plexiglas booms, the data were repeatable and represented the same values as air-dielectric booms. However that was not the case for wooden booms because of differences in the moisture, which had a direct affect on the gain. Data on metal booms was also repeatable provided the element lengths were increased to compensate for the metal boom structure.

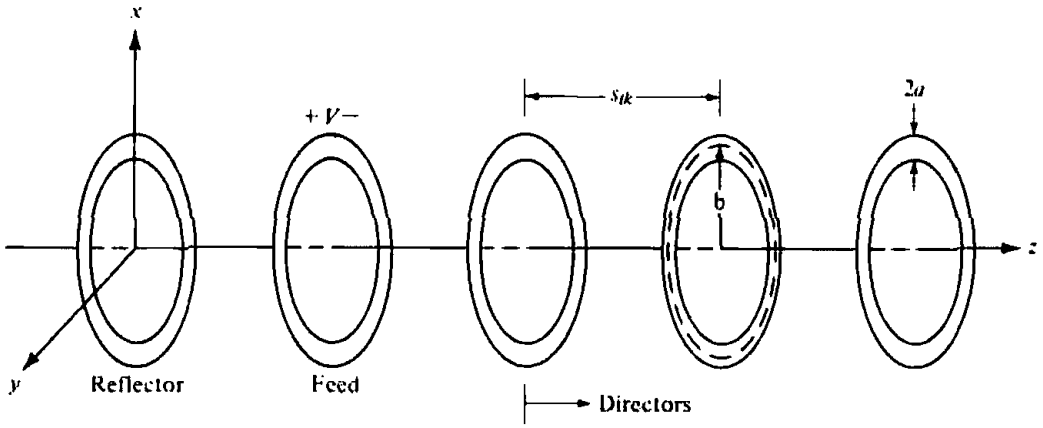


Figure 10.27 Yagi-Uda array of circular loops.

### 10.3.4 Yagi-Uda Array of Loops

Aside from the dipole, the loop antenna is one of the most basic antenna elements. The pattern of a very small loop is similar to that of a very small dipole and in the far-field region it has a null along its axis. As the circumference of the loop increases, the radiation along its axis increases and reaches near maximum at about one wavelength [31]. Thus loops can be used as the basic elements, instead of the linear dipoles, to form a Yagi-Uda array as shown in Figure 10.27. By properly choosing the dimensions of the loops and their spacing, they can form a unidirectional beam along the axis of the loops and the array.

It has been shown that the radiation characteristics of a two-element loop array, one driven element and a parasitic reflector, resulted in the elimination of corona problems at high altitudes [32]. In addition, the radiation characteristics of loop arrays mounted above ground are less affected by the electrical properties of the soil, as compared with those of dipoles [33]. A two-element loop array also resulted in a 1.8 dB higher gain than a corresponding array of two dipoles [32]. A two-element array of square loops (a feeder and a reflector) in a boxlike construction is called a "cubical quad" or simply a "quad" antenna, and it is very popular in amateur radio applications [34]. The sides of each square loop are $\lambda/4$ (perimeter of $\lambda$), and the loops are usually supported by a fiberglass or bamboo cross-arm assembly.

The general performance of a loop Yagi-Uda array is controlled by the same geometrical parameters (reflector, feeder, and director sizes, and spacing between elements), and it is influenced in the same manner as an array of dipoles [35].

In a numerical parametric study of coaxial Yagi-Uda arrays of circular loops [36] of 2 to 10 directors, it has been found that the optimum parameters for *maximum forward gain* were

1. circumference of feeder $2\pi b_2 \simeq 1.1\lambda$, where $b_2$ is its radius. This radius was chosen so that the input impedance for an isolated element is purely resistive.
2. circumference of the reflector $2\pi b_1 \simeq 1.05\lambda$, where $b_1$ is its radius. The size of the reflector does not strongly influence the forward gain but has a major effect on the backward gain and input impedance.
3. feeder-reflector spacing of about $0.1\lambda$. Because it has negligible effect on the forward gain, it can be used to control the backward gain and/or the input impedance.
4. circumference of directors $2\pi b \simeq 0.7\lambda$, where $b$ is the radius of any director and

it was chosen to be the same for all. When the circumference approached a value of one wavelength, the array exhibited its cutoff properties.

5. spacing of directors of about $0.25\lambda$, and it was uniform for all.

The radius $a$ of all the elements was retained constant and was chosen to satisfy $\Omega = 2\ln(2\pi b_2/a) = 11$ where $b_2$ is the radius of the feeder.

## References


1. C. H. Walter, *Traveling Wave Antennas*, McGraw-Hill, New York, 1965.
2. J. D. Kraus, *Electromagnetics*, McGraw-Hill Book Co., New York, 1992.
3. J. G. Brainerd, et. al., *Ultra-High-Frequency Techniques*, Van Nostrand, New York, 1942.
4. L. V. Blake, *Antennas*, John Wiley and Sons, New York, 1966.
5. G. A. Thiele and E. P. Ekelman, Jr., "Design Formulas for Vee Dipoles," *IEEE Trans. Antennas Propagat.*, Vol. AP-28, No. 4, pp. 588–590, July 1980.
6. W. L. Weeks, *Antenna Engineering*, McGraw-Hill, New York, 1968, pp. 140–142.
7. D. G. Fink (ed.), *Electronics Engineers' Handbook*, Chapter 18 (by W. F. Croswell), McGraw-Hill, New York, 1975.
8. J. D. Kraus, *Antennas*, McGraw-Hill, New York, 1988.
9. A. A. de Carvallo, "On the Design of Some Rhombic Antenna Arrays," *IRE Trans. Antennas Propagat.*, Vol. AP-7, pp. 39–46, No. 1, January 1959.
10. E. Bruce, A. C. Beck, and L. R. Lowry, "Horizontal Rhombic Antennas," *Proc. IRE*, Vol. 23, pp. 24–26, January 1935.
11. R. S. Elliott, *Antenna Theory and Design*, Prentice-Hall, Englewood Cliffs, New Jersey, 1981.
12. J. D. Kraus, "A 50-Ohm Input Impedance for Helical Beam Antennas," *IEEE Trans. Antennas Propagat.*, Vol. AP-25, No. 6, p. 913, November 1977.
13. A. G. Kandoian, "Three New Antenna Types and Their Applications," *Proc. IRE*, Vol. 34, pp. 70W–75W, February 1946.
14. S. Uda, "Wireless Beam of Short Electric Waves," *J. IEE.* (Japan), pp. 273–282, March 1926, and pp. 1209–1219, November 1927.
15. H. Yagi, "Beam Transmission of Ultra Short Waves," *Proc. IRE*, Vol. 26, pp. 715–741, June 1928. Also *Proc. IEEE*, Vol. 72, No. 5, pp. 634–645, May 1984.
16. R. M. Fishender and E. R. Wiblin, "Design of Yagi Aerials," *Proc. IEE* (London), pt. 3, Vol. 96, pp. 5–12, January 1949.
17. C. C. Lee and L.-C. Shen, "Coupled Yagi Arrays," *IEEE Trans. Antennas Propagat.*, Vol. AP-25, No. 6, pp. 889–891, November 1977.
18. H. W. Ehrenspeck and H. Poehler, "A New Method for Obtaining Maximum Gain from Yagi Antennas," *IRE Trans. Antennas Propagat.*, Vol. AP-7, pp. 379–386, October 1959.
19. H. E. Green, "Design Data for Short and Medium Length Yagi-Uda Arrays," *Elec. Engrg. Trans. Inst. Engrgs.* (Australia), pp. 1–8, March 1966.
20. W. Wilkinshaw, "Theoretical Treatment of Short Yagi Aerials," *Proc. IEE* (London), pt. 3, Vol. 93, p. 598, 1946.
21. R. J. Mailloux, "The Long Yagi-Uda Array," *IEEE Trans. Antennas Propagat.*, Vol. AP-14, pp. 128–137, March 1966.
22. D. Kajfez, "Nonlinear Optimization Reduces the Sidelobes of Yagi Antennas," *IEEE Trans. Antennas Propagat.*, Vol. AP-21, No. 5, pp. 714–715, September 1973.
23. D. Kajfez, "Nonlinear Optimization Extends the Bandwidth of Yagi Antennas," *IEEE Trans. Antennas Propagat.*, Vol. AP-23, pp. 287–289, March 1975.
24. G. A. Thiele, "Analysis of Yagi-Uda Type Antennas," *IEEE Trans. Antennas Propagat.*, Vol. AP-17, No. 1, pp. 24–31, January 1969.

25. P. A. Tirkas, Private communication.
26. G. A. Thiele, "Calculation of the Current Distribution on a Thin Linear Antenna," *IEEE Trans. Antennas Propagat.*, Vol. AP-14, No. 5, pp. 648–649, September 1966.
27. D. K. Cheng and C. A. Chen, "Optimum Spacings for Yagi-Uda Arrays," *IEEE Trans. Antennas Propagat.*, Vol. AP-21, No. 5, pp. 615–623, September 1973.
28. C. A. Chen and D. K. Cheng, "Optimum Element Lengths for Yagi-Uda Arrays," *IEEE Trans. Antennas Propagat.*, Vol. AP-23, No. 1, pp. 8–15, January 1975.
29. N. K. Takla and L.-C. Shen, "Bandwidth of a Yagi Array with Optimum Directivity," *IEEE Trans. Antennas Propagat.*, Vol. AP-25, No. 6, pp. 913–914, November 1977.
30. P. P. Viezbicke, "Yagi Antenna Design," NBS Technical Note 688, U.S. Department of Commerce/National Bureau of Standards, December 1968.
31. S. Adachi and Y. Mushiake, "Studies of Large Circular Loop Antennas," Sci. Rep. Research Institute of Tohoku University (RITU), B,9,2, pp. 79–103, 1957.
32. J. E. Lindsay, Jr., "A Parasitic End-fire Array of Circular Loop Elements," *IEEE Trans. Antennas Propagat.*, Vol. AP-15, No. 5, pp. 697–698, September 1967.
33. E. Ledinegg, W. Paponsek, and H. L. Brueckmann, "Low-Frequency Loop Antenna Arrays: Ground Reaction and Mutual Interaction," *IEEE Trans. Antennas Propagat.*, Vol. AP-21, No. 1, pp. 1–8, January 1973.
34. D. DeMaw (ed.), *The Radio Amateur's Handbook*, American Radio Relay League, p. 20-18, 56th ed., 1979.
35. A. Shoamanesh and L. Shafai, "Properties of Coaxial Yagi Loop Arrays," *IEEE Trans. Antennas Propagat.*, Vol. AP-26, No. 4, pp. 547–550, July 1978.
36. A. Shoamanesh and L. Shafai, "Design Data for Coaxial Yagi Array of Circular Loops," *IEEE Trans. Antennas Propagat.*, Vol. AP-27, No. 5, pp. 711–713, September 1979.

## *PROBLEMS*

10.1. Given the current distribution of (10-1a), show that the
(a) far-zone electric field intensity is given by (10-2a) and (10-2b)
(b) average power density is given by (10-4) and (10-5)
(c) radiated power is given by (10-11)

10.2. Determine the phase velocity (compared to free-space) of the wave on a Beverage antenna (terminated long wire) of length $l = 50\lambda$ so that the maximum occurs at angles of
(a) 10°
(b) 20°
from the axis of the wire.

10.3. The current distribution on a terminated and matched long linear (traveling wave) antenna of length $l$, positioned along the $x$-axis and fed at its one end, is given by

$$\mathbf{I} = \hat{\mathbf{a}}_x I_0 e^{-jkx'}, \quad 0 \le x' \le l$$

Find the far field electric and magnetic field components in *standard spherical coordinates*.

10.4. A long linear (traveling wave) antenna of length $l$, positioned along the $z$-axis and fed at the $z = 0$ end, is terminated in a load at the $z = l$ end. There is a nonzero reflection at the load such that the current distribution on the wire is given by

$$I(z) = I_0 \frac{e^{-jkz} + R\, e^{jkz}}{1 + R}, \quad 0 \le z \le l$$

Determine as a function of $R$ and $l$ the
(a) far-zone spherical electric field components
(b) radiation intensity in the $\theta = \pi/2$ direction

10.5. Design a Beverage antenna so that the first maximum occurs at 10° from its axis.

Assuming the phase velocity of the wave on the line is the same as that of free-space, find the
(a) lengths (exact and approximate) to accomplish that
(b) angles (exact and approximate) where the next six maxima occur
(c) angles (exact and approximate) where the nulls, between the maxima found in parts (a) and (b), occur
(d) radiation resistance using the exact and approximate lengths
(e) directivity using the exact and approximate lengths

10.6. It is desired to place the first maximum of a long wire traveling wave antenna at an angle of 25° from the axis of the wire. For the wire antenna, find the
(a) exact required length
(b) radiation resistance
(c) directivity (*in dB*)
The wire is radiating into free space.

10.7. Compute the directivity of a long wire with lengths of $l = 2\lambda$ and $3\lambda$.

10.8. A long wire of diameter $d$ is placed (in the air) at a height $h$ above the ground.
(a) Find its characteristic impedance assuming $h \gg d$.
(b) Compare this value with (10-14).

10.9. Beverage (long wire) antennas are used for over-the-horizon communication where the maximum of the main beam is pointed few degrees above the horizon. Assuming the wire antenna of length $l$ and radius $\lambda/200$ is placed horizontally parallel to the $z$-axis a height $h = \lambda/20$ above a flat, perfect electric conducting plane of infinite extent ($x$-axis is perpendicular to the ground plane).
(a) Derive the array factor for the equivalent two-element array.
(b) What is the normalized total electric field of the wire in the presence of the conducting plane?
(c) What value of load resistance should be placed at the terminating end to eliminate any reflections and not create a standing wave?

10.10. Compute the optimum directivities of a V antenna with leg lengths of $l = 2\lambda$ and $l = 3\lambda$. Compare these values with those of Problem 10.7.

10.11. Design a symmetrical V antenna so that its optimum directivity is 8 dB. Find the lengths of each leg (in $\lambda$) and the total included angle of the V (in degrees).

10.12. Repeat the design of Problem 10.11 for an optimum directivity of 5 dB.

10.13. It is desired to design a V-dipole with a maximized directivity. The length of each arm is $0.5\lambda$ (overall length of the entire V-dipole is $\lambda$). To meet the requirements of the design, what is the
(a) total included angle of the V-dipole (in degrees)?
(b) directivity (in dB)?
(c) gain (in dB) if the overall antenna efficiency is 35%?

10.14. Ten identical elements of V antennas are placed along the $z$-axis to form a *uniform broadside* array. Each element is designed to have a maximum directivity of 9 dB. Assuming each element is placed so that its maximum is also broadside ($\theta = 90°$) and the elements are spaced $\lambda/4$ apart, find the
(a) arm length of each V (in $\lambda$)
(b) included angle (in degrees) of each V
(c) approximate total directivity of the array (in dB)

10.15. Design a resonant 90° bent, $\lambda/4$ long, $0.25 \times 10^{-3}\lambda$ radius wire antenna placed above a ground plane. Find the
(a) height where the bent must be made
(b) input resistance of the antenna
(c) VSWR when the antenna is connected to a 50-ohm line

10.16. Design a five-turn helical antenna which at 400 MHz operates in the normal mode. The spacing between turns is $\lambda/50$. It is desired that the antenna possesses circular polarization. Determine the

(a) circumference of the helix (in $\lambda$ and in meters)
(b) length of a single turn (in $\lambda$ and in meters)
(c) overall length of the entire helix (in $\lambda$ and in meters)
(d) pitch angle (in degrees)

10.17. Design a five-turn helical antenna which at 300 MHz operates in the axial mode and possesses circular polarization in the major lobe. Determine the
(a) near optimum circumference (in $\lambda$ and in meters)
(b) spacing (in $\lambda$ and in meters) for near optimum pitch angle design
(c) input impedance
(d) half-power beamwidth (in degrees), first null beamwidth (in degrees), directivity (dimensionless and in dB), and axial ratio
(e) VSWR when the antenna is connected to 50- and 75-ohm coaxial lines

10.18. For Problem 10.17, plot, using the 2-D ANTENNA PATTERN PLOTTER: RECTANGULAR-POLAR computer program at the end of Chapter 2, the normalized polar amplitude pattern (in dB) assuming phasing for
(a) ordinary end-fire
(b) Hansen-Woodyard end-fire
(c) $p = 1$

10.19. For Problem 10.17, compute the directivity (in dB) using the computer program DIRECTIVITY at the end of Chapter 2 assuming phasing for
(a) ordinary end-fire
(b) Hansen-Woodyard end-fire
(c) $p = 1$
Compare with the value obtained using (10-33).

10.20. Repeat the design of Problem 10.17 at a frequency of 500 MHz.

10.21. Design an end-fire right-hand circularly polarized helix having a half-power beamwidth of 45°, pitch angle of 13°, and a circumference of 60 cm at a frequency of 500 MHz. Determine the
(a) turns needed
(b) directivity (in dB)
(c) axial ratio
(d) lower and upper frequencies of the bandwidth over which the required parameters remain relatively constant
(e) input impedance at the center frequency and the edges of the band from part (d).

10.22. Design a helical antenna with a directivity of 15 dB that is operating in the axial mode and whose polarization is nearly circular. The spacing between the turns is $\lambda/10$. Determine the
(a) Number of turns.
(b) Axial ratio, *both as an dimensionless quantity and in dB.*
(c) Directivity (in dB) based on Kraus' formula and Tai & Pereira's formula. How do they compare with the desired value?
(d) Progressive phase shifts (in degrees) between the turns to achieve the axial mode radiation.

10.23. Design a 10-turn helical antenna so that at the center frequency of 10 GHz, the circumference of each turn is $0.95\lambda$. Assuming a pitch angle of 14°, determine the
(a) mode in which the antenna operates
(b) half-power beamwidth (in degrees)
(c) directivity (in dB). Compare this answer with what you get using Kraus' formula.

10.24. A *lossless* 10-turn helical antenna with a circumference of *one-wavelength* is connected to a 78-ohm coaxial line, and it is used as a transmitting antenna in a 500-MHz spacecraft communication system. The spacing between turns is $\lambda/10$. The power in the coaxial line from the transmitter is 5 watts. Assuming the antenna is lossless:

(a) What is radiated power?
(b) If the antenna were isotropic, what would the power density (watts/m$^2$) be at a distance of 10 kilometers?
(c) What is the power density (in watts/m$^2$) at the same distance when the transmitting antenna is the 10-turn helix and the observations are made along the maximum of the major lobe?
(d) If at 10 kilometers along the maximum of the major lobe an identical 10-turn helix was placed as a receiving antenna, which was polarization-matched to the incoming wave, what is the maximum power (in watts) that can be received?

10.25. A 20-turn helical antenna operating in the axial mode is used as a transmitting antenna in a 500-MHz long distance communication system. The receiving antenna is a linearly polarized element. Because the transmitting and receiving elements are not matched in polarization, approximately how many dB of losses are introduced because of polarization mismatch?

10.26. A Yagi-Uda array of linear elements is used as a TV antenna receiving primarily channel 8 whose center frequency is 183 MHz. With a regular resonant $\lambda/2$ dipole as the feed element in the array, the input impedance is approximately 68 ohms. The antenna is to be connected to the TV using a "twin-lead" line with a characteristic impedance of nearly 300 ohms. At the center frequency of 183 MHz
(a) what should the smallest input impedance of the array be if it is desired to maintain a VSWR equal or less than 1.1?
(b) what is the best way to modify the present feed to meet the desired VSWR specifications? Be very specific in explaining why your recommendation will accomplish this.

10.27. Evaluate approximately the effect of the spacing between the director and driven element in the three-element Yagi-Uda array shown in the accompanying figure. Assume that the far-zone (radiated) field of the antenna is given by

$$E_\theta = \sin\theta \left[ 1 - e^{-j\pi/8} e^{-jks_{12}\sin\theta\sin\phi} - e^{j\pi/8} e^{+jks_{23}\sin\theta\sin\phi} \right]$$

where $s_{12}$ is the spacing between the reflector and the driven element, and $s_{23}$ is the spacing between the director and the driven element. For this problem, set $s_{12} = 0.2\lambda$ and let $s_{23} = 0.15\lambda, 0.20\lambda, 0.25\lambda$.
(a) Generate polar plots of the radiation power patterns in both $E$- and $H$-planes. Normalize the power pattern to its value for $\theta = \pi/2$ and $\phi = \pi/2$. Generate two plots, one for $E$-plane and one for $H$-plane.
(b) Compute the front-to-back ratio (FBR) in the $E$-plane given by

$$FBR|_{E-plane} = \frac{P_n\left(\theta = \frac{\pi}{2}, \phi = \frac{\pi}{2}\right)}{P_n\left(\theta = \frac{\pi}{2}, \phi = \frac{-\pi}{2}\right)}$$

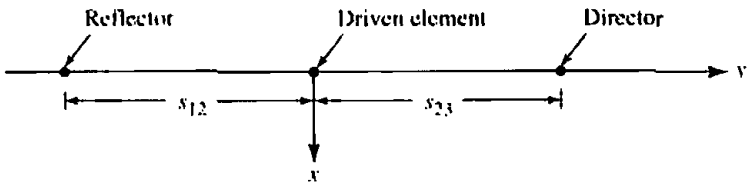


Leave your answers for both parts in terms of numbers, not dB.

10.28. Analyze a 27-element Yagi-Uda array, using the computer program YAGI-UDA ARRAY at the end of this chapter, having the following specifications:

| | |
|---|---|
| $N$ = total number of elements | = 27 |
| Number of directors | = 25 |
| Number of reflectors | = 1 |
| Total length of reflector | = $0.5\lambda$ |
| Total length of feeder | = $0.47\lambda$ |
| Total length of each director | = $0.406\lambda$ |
| Spacing between reflector and feeder | = $0.125\lambda$ |
| Spacing between adjacent directors | = $0.34\lambda$ |
| $a$ = radius of wires | = $0.003\lambda$ |

Use 8 modes for each element. Compute the
(a) far-field $E$- and $H$-plane amplitude patterns (in dB).
(b) directivity of the array (in dB).
(c) $E$-plane half-power beamwidth (in degrees).
(d) $H$-plane half-power beamwidth (in degrees).
(e) $E$-plane front-to-back ratio (in dB).
(f) $H$-plane front to back ratio (in dB).

10.29. Repeat the analysis of Problem 10.28 for a three-element array having the following specifications:

| | |
|---|---|
| $N$ = total number of elements | = 3 |
| Number of directors | = 1 |
| Number of reflectors | = 1 |
| Total length of reflector | = $0.5\lambda$ |
| Total length of feeder | = $0.475\lambda$ |
| Total length of director | = $0.45\lambda$ |
| Spacing between reflector and feeder | = $0.2\lambda$ |
| Spacing between feeder and director | = $0.16\lambda$ |
| $a$ = radius of wires | = $0.005\lambda$ |

Use 8 modes for each element.

10.30. Design a Yagi-Uda array of linear dipoles to cover all the VHF TV channels (starting with 54 MHz for channel 2 and ending with 216 MHz for channel 13. See Appendix IX). Perform the design at $f_0$ = 216 MHz. Since the gain is not affected appreciably at $f < f_0$, as Figure 10.24 indicates, this design should accommodate all frequencies below 216 MHz. The gain of the antenna should be 14.4 dB (above isotropic). The elements and the supporting boom should be made of aluminum tubing with outside diameters of $\frac{3}{8}$ in. (≃ 0.95 cm) and $\frac{3}{4}$ in. (≃ 1.90 cm), respectively. Find the number of elements, their lengths and spacings, and the total length of the array (in $\lambda$, meters, and feet).

10.31. Repeat the design of Problem 10.30 for each of the following:
(a) VHF-TV channels 2–6 (54–88 MHz. See Appendix IX)
(b) VHF-TV channels 7–13 (174–216 MHz. See Appendix IX)

10.32. Design a Yagi-Uda antenna to cover the entire FM band of 88–108 MHz (100 channels spaced at 200 KHz apart. See Appendix IX). The desired gain is 12.35 dB (above isotropic). Perform the design at $f_0$ = 108 MHz. The elements and the supporting boom should be made of aluminum tubing with outside diameters of $\frac{3}{8}$ in. (≃ 0.95

cm) and $\frac{3}{4}$ in. ($\simeq$ 1.90 cm), respectively. Find the number of elements, their lengths and spacings, and the total length of the array (in $\lambda$, meters, and feet).

10.33. Design a Yagi-Uda antenna to cover the UHF TV channels (512–806 MHz. See Appendix IX). The desired gain is 12.35 dB (above isotropic). Perform the design at $f_0 = 806$ MHz. The elements and the supporting boom should be made of wire with outside diameters of $\frac{3}{32}$ in. ($\simeq$ 0.2375 cm) and $\frac{1}{16}$ in. ($\simeq$ 0.475 cm), respectively. Find the number of elements, their lengths and spacings, and the total length of the array (in $\lambda$, meters, and feet).

## *COMPUTER PROGRAM - YAGI-UDA ARRAY*

```
C***********************************************************************
C THIS IS A FORTRAN PROGRAM THAT COMPUTES, FOR THE YAGI-UDA
C ANTENNA ARRAY, THE:
C
C   I.  FAR-ZONE E- AND H-PLANE AMPLITUDE PATTERNS (in dB)
C   II.  DIRECTIVITY OF THE ARRAY (in dB)
C   III. E-PLANE HALF-POWER BEAMWIDTH (in degrees)
C   IV. H-PLANE HALF-POWER BEAMWIDTH (in degrees)
C   V.  E-PLANE FRONT-TO-BACK RATIO (in dB)
C   VI. H-PLANE FRONT-TO-BACK RATIO (in dB)
C
C THE PROGRAM IS BASED ON POCKLINGTON'S INTEGRAL
C EQUATION FORMULATION OF SECTION 10.3.3, EQUATIONS
C (10-42) - (10-65a). M ENTIRE DOMAIN COSINUSOIDAL (FOURIER)
C BASIS MODES ARE USED FOR EACH OF THE ANTENNA
C ELEMENTS.
C
C
C       **INPUT PARAMETERS
C       1. M     = NUMBER OF ENTIRE DOMAIN BASIS MODES
C       2. N     = NUMBER OF ANTENNA ELEMENTS
C       3. L     = LENGTH OF EACH ELEMENT l_n (in λ)
C       4. ALPHA = RADIUS OF EACH ELEMENT a (in λ)
C       5. S     = SEPARATION BETWEEN THE ELEMENTS s_n (in λ)
C
C       **NOTES
C       1. REFER TO FIGURE 10.17 FOR THE GEOMETRY.
C       2. DRIVEN ELEMENT IS AT THE ORIGIN.
C       3. FIRST ELEMENT (N = 1) IS THE FIRST DIRECTOR.
C       4. REFLECTOR IS THE N-1 ELEMENT; ONLY ONE REFLECTOR.
C       5. DRIVEN ELEMENT IS N.
C       6. THE RADIUS OF ALL THE ELEMENTS IS THE SAME.
C
C***********************************************************************
```